Convection in Lorenz's global energy cycle with the ECMWF model

Martin Steinheimer[1], Michael Hantel[1] and Peter Bechtold

Research Department

[1]Department of Meteorology and Geophysics, University of Vienna, Vienna, Austria

European Centre for Medium-Range Weather Forecasts
Europäisches Zentrum für mittelfristige Wettervorhersage
Centre européen pour les prévisions météorologiques à moyen terme

Abstract

Lorenz's global energy cycle includes the conversion rate C between available potential and kinetic energy. In traditional estimates of C only gridscale processes were evaluated; sub-gridscale processes were lumped into dissipation. It is argued that this is inadequate; organized sub-gridscale heat fluxes like deep convection cannot be treated as molecular.

Here both C^{grid} and C^{sub} are evaluated from the ECMWF Integrated Forecast System (IFS), for a one year forecast in climate mode. The sub-gridscale fluxes are obtained from the model parametrization and the results tested for consistency; the largest contribution comes from the convection scheme. The integrand of C^{sub}, the familiar *buoyancy flux* $-\overline{\alpha'\omega'}$, is locally much smaller than its gridscale counterpart $-\overline{\alpha}\,\overline{\omega}$. However, the buoyancy flux is upward throughout, and thus representative for, the global atmosphere. The global annual means are $C^{grid}=(3.4\pm0.1)$W/m^2 and $C^{sub}=(1.7\pm0.1)$W/m^2. Further, the gridscale generation rate of available potential energy is evaluated independently and found to be $G^{grid}=(3.0\pm0.2)$W/m^2.

These results suggest that (i) the sub-gridscale processes contribute significantly to the Lorenz energy cycle, and (ii) the cycle, represented by the total dissipation of $D=(5.1\pm0.2)$W/m^2, is more intense than all earlier gridscale estimates have indicated.

1   Introduction

The concept of available potential energy of Lorenz (1955) describes the global energy cycle with the ultimate goal of quantifying the intensity of the general circulation of the atmosphere. However, only gridscale data have been used so far for evaluating the intensity of the circulation. Turbulent processes, including the important mechanisms of organized convection, have not been considered of any significance for the global energy cycle and thus have almost never been incorporated into the Lorenz exchange fluxes. It is the purpose of this study to provide evidence that sub-gridscale processes are of about the same relevance for the global energetics as are the traditional gridscale fluxes. The result will be that the global cycle is about twice as intense as thought so far.

The Lorenz energy cycle involves the reservoirs of available potential energy and kinetic energy, together with the related sources and sinks. The source for the available potential energy is the generation rate (G), while the kinetic energy is fed by the conversion rate (C) from available potential into kinetic energy, and diminished by the dissipation rate (D). All these quantities are understood as global climatological means. This implies that the reservoirs of available potential and kinetic energy are stationary. Hence, the fluxes G, C and D should be equal. The intensity of the general circulation can be specified by evaluating one of these global mean flux quantities.

Classical data evaluations (Oort, 1964; Oort, 1983; Oort and Peixóto, 1983; Arpe et al., 1986; Peixóto and Oort, 1992) estimated C from gridscale data. G was also estimated, through employing the atmospheric heating rate and the efficiency factor, from gridscale data. The sub-gridscale effects were considered as molecular and lumped into dissipation. One prominent reason for this simplification was of a practical nature: The coarse data fields available for the early studies did not allow for the evaluation of sub-gridscale turbulent fluxes.

This state of affairs remained effective essentially up to today. The basic philosophy in all existing numerical studies based on the Lorenz theory is that sub-gridscale processes do not need to be explicitly considered. This attitude has not changed in the meantime although sub-gridscale budget data have long become available. Even in the more recent model and data evaluation studies the role of the sub-gridscale component in the global energy budget is not mentioned (e.g., Siegmund, 1994; Rosen, 1999; Li et al., 2007).

In order to quantitatively calculate the source, conversion and sink rates, which are global integrals in the Lorenz cycle, the first logical step is to diagnose the *local patterns* of the corresponding integrands. These can only be available in form of quantities on a grid, i.e., as quantities representative as averages over the corresponding grid cell, specified by the 3D space-resolution and the time resolution of the data available; in the experiment of this study this is about 125 km in horizontal direction, 0.2-40 hPa in vertical direction, and about 1/2 hour in time. Thus the second logical step is to discuss, not only the local energy equations that shall be applied for the budgets, but also the role of the *finite grid size* and, as far as nonlinear terms are involved, the corresponding correlation quantities over the grid cell which eventually show up as sub-gridscale quantities in the budget equations. The third logical step is then to calculate the *global integrals* of the diagnosed gridscale quantities in order to come up with estimates of the familiar global fluxes characteristic for the Lorenz energy cycle.

Looking at the local gridscale ($-\overline{\alpha}\,\overline{\omega}$) and sub-gridscale ($-\overline{\alpha'\omega'}$) conversion rates, which will be introduced in Section 3 and are the integrands of the global mean conversion rate C, reveals that $-\overline{\alpha'\omega'}$ is locally negligible in size compared to $-\overline{\alpha}\,\overline{\omega}$. This has been a further argument in favor of neglecting the small term $-\overline{\alpha'\omega'}$ altogether (T. Hollingsworth, personal communication). The large gridscale $-\overline{\alpha}\,\overline{\omega}$, sometimes referred to as *adiabatic term* (e.g., Bhatla et al., 2004), is positive in the tropics and negative in the subtropics, representing the Hadley cells on both hemispheres. These minima and maxima cancel each other almost completely in the global mean. In contrast, the locally quite small $-\overline{\alpha'\omega'}$ is positive practically throughout the entire atmosphere and thus suffers no cancelation. Following Haimberger and Hantel (2000) and Hantel et al. (2001) the quantity $-\overline{\alpha'\omega'}$ will also be referred to as the *buoyancy flux*.

Since high quality data from reanalysis projects carried out by NCEP/NCAR (Kalnay et al., 1996) and ECMWF (Uppala et al., 2005) have become available there should be no further need for excluding the integral of the buoyancy flux from the global energy budget. The time seems to be ripe for completing Lorenz's energy cycle through explicit implementation of the sub-gridscale processes. A first attempt into this direction has been made by Hantel and Haimberger (2000) and Haimberger and Hantel (2000), in the sequel cited as HH-I, HH-II. In these studies both generation rate G and conversion rate C were split into a gridscale (G^{grid}, C^{grid}) and a sub-gridscale fraction (G^{sub}, C^{sub}); the grid scale fractions correspond to Lorenz's classical G and C. Concerning the dissipation rate D it was assumed that dissipation occurs only on the smallest scales and thus is completely described by D^{sub} while D^{grid} should be close to zero.

The evaluations of HH-II suggest that the sub-gridscale conversion rate C^{sub} is of about equal size as the gridscale conversion rate C^{grid}. This implies that the global energy cycle is about twice as efficient as has been known from the classical evaluations. Figure 1 presents the results achieved by HH-II. The reason why HH-II focused strongly on the conversion rate was that evaluating the two components of C is a quite transparent task, as opposed to G which is more involved. The local fields $-\overline{\alpha}\,\overline{\omega}$ and $-\overline{\alpha'\omega'}$ can principally be diagnosed today so that the corresponding global averages C^{grid} and C^{sub} can be determined by straight integration. The present study will also primarily be focused on these two components of the conversion rate C. Conversely, of the two components of the generation rate only the gridscale component G^{grid} can be evaluated while the sub-gridscale component G^{sub} cannot.

The studies HH-I, HH-II were limited by the fact that the sub-gridscale conversion rate had to be estimated with a quite preliminary method. Consequently the estimates of HH-II had an error of almost 80% for C^{sub}.

The method adopted in the present study is to draw the gridscale quantities required from ECMWF's weather prediction model IFS (Integrated Forecast System). Further, the most relevant sub-gridscale quantities that hitherto have been missing in the Lorenz's energy cycle will be inferred from the parametrization schemes of the IFS. This can be made in a consistent manner and with much improved accuracy.

The data used in this study will be extracted from a one year forecast in climate mode of the IFS started from 1 August 2000. The routinely stored fields as well as special fields from the parametrization schemes will be

employed. While $-\overline{\alpha}\,\overline{\omega}$ is explicitly contained in the model's temperature budget equation and can be calculated from gridscale fields, $-\overline{\alpha'\omega'}$ is neglected in the temperature budget equation of the IFS. However, the buoyancy flux can be calculated from the sub-gridscale fluxes of temperature and specific humidity (Section 3). The divergences of these fluxes play an important role in the forecast equations of temperature and specific humidity and are therefore explicitly included in the parametrization of the model. How these fluxes are extracted from the corresponding schemes is presented in Section 4. The pertinent details of the model run are presented in Section 5.

In his consideration of the cumulus parametrization problem Arakawa (2004) discusses the notion pairs gridscale/subgrid-scale and resolved/unresolved as opposed to large scale/cumulus scale and observed/non-observed. He points out that in diagnostic studies of cumulus effects based on observed large-scale budgets (e.g., Yanai and Johnson, 1993) the density of the observation network separates observed and non-observed processes and maintains that 'finding a cause-and-effect relationship should not be an issue' in such a study. This is exactly the philosophy of the present investigation. The parameterized fluxes of the IFS will be used as substitutes for the unobserved sub-gridscale (in short: convective) processes in the atmosphere. While the convective processes go unobserved they nevertheless have a deep impact, not only upon the forecast fields, but upon the global energy budget as well. To extract them from the IFS is a matter of practical convenience. However, no statement concerning a possible cause-and-effect relationship is intended in the present study.

This will be advantageous from another perspective: The notion *sub-gridscale* comprises processes that are so different as are anisotropic penetrative cumulus convection and isotropic boundary layer convection. As again Arakawa (2004) points out the statistical distributions of dynamical and thermodynamical properties of air in the cloudy atmosphere are highly skewed; following Arakawa, the concepts of *mean and variance* are less useful than those of *environment and cloud*. While the latter distinction is indispensable when it comes to closure and parametrization the formal notion pair mean/variance, expressed here as gridscale/sub-gridscale, is the only way to lump physically different unresolved processes into one unifying category.

The straightforward 'mean-and-variance' method will nevertheless reveal that the sub-gridscale buoyancy flux is most pronounced in the latitudes of the intertropical convergence zone (ITCZ) where penetrative cumulus convection is dominant; the buoyancy flux is less dominant, while still relevant, in the boundary layer where convection tends to be isotropic. Both mechanisms are physically different. Yet both are of *convective* nature and both are controlled by buoyancy; thus it may seem admissible to apply the notion *sub-gridscale* in equal manner for both.

The use of the parameterized output does not necessarily reproduce the energy budget of the IFS. For example, the interaction between sub-gridscale potential and eddy kinetic energy through the buoyancy flux, a key process in the turbulence kinetic energy equation (Stull, 1988), is actually not reproduced in the present implementation of the IFS. This does however not prevent the IFS to be energetically consistent, since only the gridscale energy reservoirs are considered in the model.

Finally, no attempt will be made in this paper to advance in any way the physical background of Lorenz's energy cycle. There have been various studies in the past that have investigated further aspects of a sometimes deep theoretical background to the Lorenz theory. For example, Johnson (2000) considers in his review article (see also citations therein) the relations between the energy budget and the entropy budget and points to a widespread misconception 'that available potential energy, once generated, is the spring which drives atmospheric circulations'. The present study does not try to get involved in these discussions but will be satisfied with accepting the global energy budget in the classical form Lorenz gave it. The only innovative aspect will be to discuss the convective component. This component has been implicitly contained in the Lorenz cycle from the beginning but has been tacitly suppressed by practically all subsequent data evaluations. The key purpose of this study is to diagnose this missing component and to demonstrate its relevance.
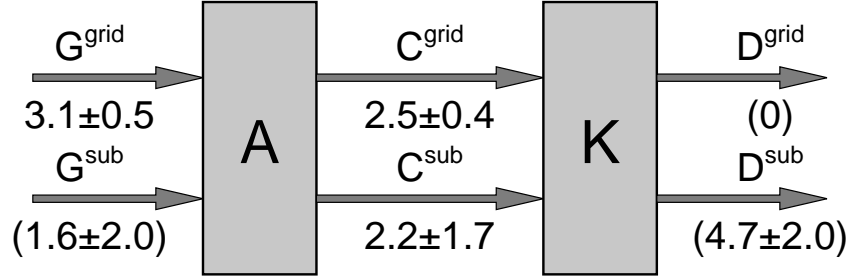
Figure 1: Lorenz's global energy cycle generalized to include sub-gridscale processes. K and A are the reservoirs of available potential and kinetic energy, respectively. The traditional gridscale conversion rates are denoted G^{grid}, C^{grid} and D^{grid}. The corresponding new sub-gridscale conversion rates are G^{sub}, C^{sub} and D^{sub}. Values estimated assuming stationary reservoirs A and K are printed in parentheses (redrawn from Haimberger and Hantel, 2000).

2   Local energy equations

Since total energy cannot objectively be separated into parts (van Mieghem, 1973, Falk and Ruppel, 1976) the separation of total energy into kinetic and internal energy is ambiguous. The same applies to the exchange between these arbitrarily chosen energy forms. In HH-I three equivalent sets of local equations of thermodynamic and mechanical energy were discussed; the authors decided that the most useful for numerical evaluation is the one suggested by Lorenz (1967). Using standard cartesian tensor notation (T = temperature, p = pressure, α = specific volume, $\omega = dp/dt$, Φ = geopotential, k = 3D-kinetic energy, π_{ij} = tensor of molecular momentum flux, ε = local dissipation, s = specific entropy, $Q = T ds/dt$ = net heating, c_p = specific heat at constant pressure) this set of equations reads:

$$\frac{\mathrm{d}a}{\mathrm{d}t} = NQ + \alpha\omega \tag{1}$$

$$\frac{\mathrm{d}b}{\mathrm{d}t} + \alpha\frac{\partial}{\partial x_j}(pv_j + \pi_{ij}v_i) = \varepsilon - \alpha\omega \tag{2}$$

The state quantities are defined as:

$$a \equiv Nc_pT + P \tag{3}$$

$$b \equiv k + \Phi - p\alpha \tag{4}$$

Definition of the efficiency factor N follows Lorenz (1967) and Boer (1975):

$$N \equiv 1 - (p_r/p)^\kappa \tag{5}$$

$$\frac{\mathrm{d}N}{\mathrm{d}t} = -\kappa(1-N)\left(\frac{1}{p_r}\frac{\mathrm{d}p_r}{\mathrm{d}t} - \frac{\omega}{p}\right) \tag{6}$$

p_r is a barotropic reference pressure chosen otherwise arbitrarily except for the condition that the global mean of N is zero; $\kappa = R_a/c_p$ (R_a = gas constant of dry air). The potential P is a function of potential temperature θ specified by:

$$\mathrm{d}P(\theta) = R_a \theta \left[\frac{p_r(\theta)}{p_0}\right]^\kappa \frac{1}{p_r(\theta)} \mathrm{d}p_r(\theta) \tag{7}$$

For this set of equations the local conversion rate between kinetic and potential energy is the flux $-\alpha\omega$, on the gridscale to be understood as $-\overline{\alpha\omega}$. The gridscale adiabatic term $-\overline{\alpha}\,\overline{\omega}$ can be calculated from gridscale data archived operationally by GCMs (global circulation models) but the sub-gridscale buoyancy flux $-\overline{\alpha\,'\omega'}$ is not available. However, this correlation quantity, by substituting α using the gas law and virtual temperature T_v, can be trasnformed into:

$$-\overline{\alpha'\omega'} = -\left[\frac{R_a}{p} + \frac{(R_v - R_a)\overline{q_v}}{p}\right]\overline{T'\omega'} - \frac{(R_v - R_a)\overline{T}}{p}\overline{q_v'\omega'} \tag{8}$$

R_v is the gas constant of water vapor and q_v is specific humidity. The liquid water fraction of the air was neglected as well as pressure perturbations and triple correlations. Following Hantel et al. (1993) the turbulent fluxes of sensible heat ($w = c_p g^{-1} \overline{T'\omega'}$) and latent heat ($f = L_v g^{-1} \overline{q_v'\omega'}$, L_v=condensation heat) are introduced. This turns Eq. (8) into:

$$-\overline{\alpha'\omega'} = -\frac{g}{p}\left[\frac{R_a}{c_p} + \frac{(R_v - R_a)\overline{q_v}}{c_p}\right]w - \frac{g}{p}\frac{(R_v - R_a)\overline{T}}{L_v}f \tag{9}$$

To diagnose the buoyancy flux with this formula the turbulent fluxes w and f can be taken from diagnosed gridscale budgets as has been done in HH-II, or extracted from parametrization as done in this study.

In HH-II the budget equation of moist enthalpy was used to diagnose the *total convective heat flux* ($c = w + f$) from reanalysis data of NCEP/NCAR (Kalnay et al., 1996) and ECMWF (Uppala et al., 2005). To get the fluxes w and f separately, the Bowen ratio (w/f) was specified externally. This closure assumption has been the drawback of the method used in HH-II. The specification of the Bowen ratio profile is largely arbitrary, since neither this quantity nor w or f separately are routinely observed.

A further point in HH-II was how to diagnose the integrand of the generation rate. For this purpose the Lorenz net heating was equated to the *response*, a quantity defined as follows:

$$Q = \frac{\mathrm{d}c_p T}{\mathrm{d}t} - \alpha\omega = R \tag{10}$$

The heating $Q = T\mathrm{d}s/\mathrm{d}t$ comprises reversible and irreversible contributions from the processes of radiation, phase changes, dissipation (due to local velocity gradients), heat conduction (due to local temperature gradients) and diffusion (due to local concentration gradients). However, it has been impossible to estimate Q from these actual physical processes; the reason is that this approach would be too inaccurate (see, e.g., the early attempts by Newell et al., 1970). Rather, Q has been estimated in HH-II from the dry enthalpy equation (10) in form of

the *response R*. This quantity is defined on the gridscale as follows:

$$\overline{R} = \underbrace{c_p \frac{\partial \overline{T}}{\partial t} + c_p \nabla_2 \cdot \overline{T} \, V_2 + c_p \frac{\partial \overline{T} \overline{\omega}}{\partial p} - \overline{\alpha} \, \overline{\omega}}_{\overline{R}^{grid}} + \underbrace{c_p \frac{\partial \overline{T' \omega'}}{\partial p} - \overline{\alpha' \omega'}}_{\overline{R}^{sub}}. \tag{11}$$

This setting will enable us to estimate the components $\overline{R}^{grid}$, $\overline{R}^{sub}$ of the generation rate[1].

3 Conversion and generation rates

From the local quantities the corresponding global generation and conversion fluxes as defined by Lorenz are gained as global mass averages (indicated by curly brackets in this paper). This yields the global conversion rate $C = \{-\alpha\omega\}$. If the conversion rate is split into a local average (denoted by an overbar) over a pertinent space/time interval (one gridbox in the model) and the deviation from this mean (indicated by a prime) its global mass average yields:

$$C = C^{grid} + C^{sub} = \left\{ -\overline{\alpha} \, \overline{\omega} \right\} + \left\{ -\overline{\alpha' \omega'} \right\} \tag{12}$$

Despite the limitations of the method applied in HH-II, this study nevertheless demonstrated successfully that C^{sub} is positive and not negligible in size compared to C^{grid}. The diagnosed results of this preliminary work, with an estimated error of about 80 % for C^{sub}, are reproduced in Fig. 1.

With the concept of the response R the generation rate components are defined as:

$$G^{grid} = \overline{N} \, \overline{R}; \qquad G^{sub} = \overline{N' R'} \tag{13}$$

Since both $\overline{N}$ and $\overline{R}$ can be extracted from model data, the gridscale conversion rate G^{grid} is readily accessible and has been included in Fig. 1. On the other hand, neither N' nor R' are accessible from model data and thus, as already noted by HH-II, G^{sub} cannot be independently diagnosed.

In the early evaluations of the Lorenz global cycle the conversion rate was not calculated in the '$\alpha\omega$–formulation' but in the hydrostatically equivalent 'V gradΦ–formulation' (e.g., Oort and Rasmusson, 1971; Peixóto and Oort, 1992). This seems to be an issue even in recent evaluations (e.g., Li et al., 2007). For selected cases (not shown in detail here) both formulations were applied; it was found that, for the global average, both yield identical results within error margins. For this reason the 'V gradΦ–formulation' was abandoned; the '$\alpha\omega$–formulation' was exclusively employed.

---

[1]Note: $\overline{T' \omega'}$ is zero at the surface. It diverges in the less than 1 cm thick skin layer above the surface. The molecular sensible heat flux converges from the surface flux to zero at the top of the skin layer (cf. HH-II). This distinction is only relevant for the calculation of $\overline{R}^{sub}$, while otherwise the molecular sensible heat flux is included in w.

4 Isolating the buoyancy flux from the IFS

In order to gain the buoyancy flux by means of Eq. (9) the central task is to extract w and f from the IFS. The gridscale forecast equations are discussed first, followed by the parameterized tendencies involved.

4.1 The forecast equations

Gridscale state quantities, carried in the IFS as prognostic variables, are, among others, temperature $\overline{T}$, specific humidity $\overline{q_v}$, and cloud water $\overline{q_{li}}$ (indices l, i for liquid water and ice). The tendencies of the first two are gained from the following forecast equations in η-coordinates (Ritchie et al., 1995):

$$
\frac{\partial \overline{T}}{\partial t} = -\left(\overline{V}_2 \cdot \nabla_2 \overline{T} + \overline{\dot{\eta}} \frac{\partial \overline{T}}{\partial \eta} - \frac{\overline{\alpha} \, \overline{\omega}}{c_p} \right) + P_T + K_T \tag{14}
$$

$$
\frac{\partial \overline{q_v}}{\partial t} = -\left(\overline{V}_2 \cdot \nabla_2 \overline{q_v} + \overline{\dot{\eta}} \frac{\partial \overline{q_v}}{\partial \eta} \right) + P_q + K_q \tag{15}
$$

Notation is standard, the index 2 denotes horizontal wind and horizontal nabla operator. P_T and P_q comprise the contributions of the parametrization; K_T and K_q stand for horizontal diffusion. In the current model implementation no horizontal diffusion is applied to specific humidity, hence K_q is neglected and will be dropped from here on. Further, in the present experiment K_T was stored, together with other terms, in the quantity $\partial T/\partial t|_{remain}$ (see Tab. 2), so K_T will not be explicitly visible in the subsequent equations. Likewise the small buoyancy flux $-\overline{\alpha'\omega'}$ does not explicitly show up in Eq. (14) because it is for the most part balanced by dissipation which is included in P_T in a correspondingly reduced form.

The terms in parentheses are understood as advection in spherical coordinates with vertical hybrid coordinate η (Simmons and Burridge, 1981). The advection is calculated using a semi-Lagrangian method and the thermodynamic equation (14) is solved semi-implicitly. For details of the algorithm see Ritchie et al. (1995) and Hortal (2002).

The terms P_T and P_q are split into apparent tendencies from the various parametrization schemes in the IFS (diffusion $diff$, convection $conv$, cloud $cloud$, and radiation rad)[2]:

$$
P_T = \left.\frac{\partial T}{\partial t}\right|_{diff} + \left.\frac{\partial T}{\partial t}\right|_{conv} + \left.\frac{\partial T}{\partial t}\right|_{cloud} + \left.\frac{\partial T}{\partial t}\right|_{rad} \tag{16}
$$

$$
P_q = \left.\frac{\partial q_v}{\partial t}\right|_{diff} + \left.\frac{\partial q_v}{\partial t}\right|_{conv} + \left.\frac{\partial q_v}{\partial t}\right|_{cloud} \tag{17}
$$

The temperature tendency due to gravity wave drag processes used to be calculated in a separate scheme in the IFS. However, effective since the IFS Cycle 31R1, a common solver for temperature diffusion and turbulent orographic form drag (gravity wave drag) has been introduced. The buoyancy flux will be gained by extracting the turbulent heat flux w from (16) and the turbulent heat flux f from (17) and substituting w and f into Eq. (9).

---

[2]The expression "diffusion scheme", often used in daily parlance, comprises not only molecular diffusion but includes also massflux contributions and dissipation. Its full name reads "turbulent transport and interaction with the surface" (ECMWF, 2007). For simplicity the subscript *"diff"* in Eqs. (16), (17) will be kept here.

The last term in (16) describe the heat sources due to radiation; it acts only upon temperature, not upon specific humidity or condensate.

4.2 Apparent tendencies in the IFS

The model equations (14), (15) can now be recast in the following symbolic form:

$$\frac{\partial \overline{T}}{\partial t} = \left.\frac{\partial T}{\partial t}\right|_{dyn} + P_T \tag{18}$$

$$\frac{\partial \overline{q_v}}{\partial t} = \left.\frac{\partial q_v}{\partial t}\right|_{dyn} + P_q \tag{19}$$

The gridscale tendencies on the left are composed of the contributions of the gridscale processes (subscript *dyn* for 'dynamic terms', equivalent to the quantities in parentheses in the forecast equations) and of the contributions P_T, P_q of non-gridscale processes to be parameterized according to Eqs. (16), (17).

It should be stressed that only the left sides of these equations are real tendencies like, for example, the partial derivative of $\overline{T}$ with respect to time. The terms on the right of Eqs. (18), (19), on the other hand, represent different contributions to the tendencies which, however, are no tendencies by themselves. This has been indicated by suppressing the overbar on the terms on the right sides. For example, there is no quantity like T_{dyn} that could be gained by independently integrating $(\partial T/\partial t)|_{dyn}$ with respect to time. Rather, the expression $(\partial T/\partial t)|_{dyn}$ is to be considered as an *apparent tendency*. Each one of these apparent tendencies in Eqs. (18), (19) is a shorthand notation for the complex processes that yield a certain contribution to the true tendency $\partial \overline{T}/\partial t$ of the gridscale state quantity $\overline{T}$.

These processes can be of a quite different nature. For example, the processes represented by $(\partial T/\partial t)|_{dyn}$ describe transformations of gridscale quantities; on the other hand, the processes represented by P_T, P_q specified in Eqs. (16), (17) describe parameterizations of sub-gridscale contributions.

4.3 Calculating the turbulent fluxes

The ECMWF parametrization involves, among other processes not discussed here, phase changes and turbulent fluxes. The phase changes are transformations between reservoirs of state quantities and require careful observation of budget laws. The turbulent fluxes, on the other hand, are the ones to be isolated. This complex parametrization task is implemented in the IFS in form of the following schemes (ECMWF, 2007):

- The *diffusion scheme* models boundary-layer and free atmospheric vertical diffusion, transport and microphysics in stratocumulus clouds, as well as kinetic energy dissipation through gravity wave and surface drag.

- The *convection scheme* calculates convective cloud and transport processes. In addition, it communicates with the stratiform cloud scheme through the detrainment of cloud water and ice.

- The *cloud scheme* computes cloud fraction, precipitation and microphysical phase changes in stratiform clouds; no turbulent fluxes are included.

For the exchange between the state quantities specific humidity $\overline{q_v}$, cloud water $\overline{q_l}$, $\overline{q_i}$ and precipitation water $\overline{q_r}$, $\overline{q_s}$ there are four phase change terms in each corresponding budget equation. These generate eight heating terms in the temperature equation. Four are caused by condensation/sublimation of water vapour and the remaining four are caused by the freezing/melting transition from q_l to q_i, q_s and from q_r to q_i, q_s. They will be included in the temperature equation through the two terms with the superscripts $v\leftrightarrow lirs$ (four phase fluxes between vapor and condensed water) and $lr\leftrightarrow is$ (another four phase fluxes between the liquid and the frozen phase of water). This reads for the diffusion scheme and the convection scheme in the temperature forecast equation:

$$\frac{\partial T}{\partial t}\bigg|_{diff} = \frac{\partial T}{\partial t}\bigg|_{diff}^{turb} + \frac{\partial T}{\partial t}\bigg|_{diff}^{v\leftrightarrow lirs} + \frac{\partial T}{\partial t}\bigg|_{diff}^{lr\leftrightarrow is} + \frac{\partial T}{\partial t}\bigg|_{diff}^{diss} + \frac{\partial T}{\partial t}\bigg|_{diff}^{gw} ; \tag{20}$$

$$\frac{\partial T}{\partial t}\bigg|_{conv} = \frac{\partial T}{\partial t}\bigg|_{conv}^{turb} + \frac{\partial T}{\partial t}\bigg|_{conv}^{v\leftrightarrow lirs} + \frac{\partial T}{\partial t}\bigg|_{conv}^{lr\leftrightarrow is} ; \tag{21}$$

and for gaseous specific humidity:

$$\frac{\partial q_v}{\partial t}\bigg|_{diff} = \frac{\partial q_v}{\partial t}\bigg|_{diff}^{turb} + \frac{\partial q_v}{\partial t}\bigg|_{diff}^{v\leftrightarrow lirs} ; \tag{22}$$

$$\frac{\partial q_v}{\partial t}\bigg|_{conv} = \frac{\partial q_v}{\partial t}\bigg|_{conv}^{turb} + \frac{\partial q_v}{\partial t}\bigg|_{conv}^{v\leftrightarrow lirs} . \tag{23}$$

Note that the phase fluxes $lr\leftrightarrow is$ concern only the apparent tendency of temperature. The cloud scheme contains no turbulent contribution and thus does not need to be discussed here (see the list in Appendix A).

Contributions to the apparent tendencies due to turbulence come from the diffusion and the convection scheme (not from the cloud scheme). This yields:

$$\frac{\partial T}{\partial t}\bigg|^{turb} = \frac{\partial T}{\partial t}\bigg|_{diff}^{turb} + \frac{\partial T}{\partial t}\bigg|_{conv}^{turb}$$
$$\frac{\partial q_v}{\partial t}\bigg|^{turb} = \frac{\partial q_v}{\partial t}\bigg|_{diff}^{turb} + \frac{\partial q_v}{\partial t}\bigg|_{conv}^{turb} . \tag{24}$$

The convective contributions are by far the largest ones; the diffusive terms are generally much smaller. Yet the diffusive terms can for principal reasons not be neglected; they couple the free atmosphere fluxes to the molecular heat exchange across the earth's surface and, when neglected, cause severe inconsistencies in the fluxes of sensible and latent heat.

The parameterized tendencies in the IFS can be interpreted in the sense that the only components that contribute to the sub-gridscale fluxes w, f are the four apparent tendencies with superscript *turb*; they are represented in Eq. (24). Thus the first step to obtain w, f from the tendencies is to define the *kinematic turbulent temperature fluxes* F_{diff}^T, F_{conv}^T through:

$$-g\frac{\partial F_{diff}^T}{\partial p} = \frac{\partial T}{\partial t}\bigg|_{diff}^{turb} ; \qquad -g\frac{\partial F_{conv}^T}{\partial p} = \frac{\partial T}{\partial t}\bigg|_{conv}^{turb} \tag{25}$$

In similar manner *the kinematic turbulent moisture fluxes* $F_{diff}^{q_v}$, $F_{conv}^{q_v}$ are defined through:

$$-g\frac{\partial F_{diff}^{q_v}}{\partial p} = \left.\frac{\partial q_v}{\partial t}\right|_{diff}^{turb}; \qquad -g\frac{\partial F_{conv}^{q_v}}{\partial p} = \left.\frac{\partial q_v}{\partial t}\right|_{conv}^{turb} \tag{26}$$

The fluxes F are gained from the corresponding tendencies, which are functions of pressure, through straight vertical mass integration plus observing that there is no material flux across the top of the atmosphere ($p=0$), e.g.:

$$F_{diff}^{T}(p) = -\frac{1}{g}\int_{p'=0}^{p'=p}\left(\left.\frac{\partial T}{\partial t}\right|_{diff}^{turb}\right)\mathrm{d}p' \tag{27}$$

From the kinematic fluxes the convective heat and moisture fluxes are obtained as:

$$w(p) = c_p\left(F_{diff}^{T} + F_{conv}^{T}\right); \quad f(p) = L_v\left(F_{diff}^{q_v} + F_{conv}^{q_v}\right) \tag{28}$$

Both w and f, like the kinematic fluxes, are functions of pressure within the column over which the mass integration (27) has been carried out. In addition, of course, all are functions of time and of the position of the column, i.e., of the horizontal coordinates.

Figs. 2, 3 show the kinematic fluxes F_{conv}^{T}, $F_{conv}^{q_v}$, F_{diff}^{T}, $F_{diff}^{q_v}$ and their respective sums for the month of April. These represent the basic information required for diagnosing the field of the buoyancy flux. Only the two that are yielded by the convection scheme are explicitly available: F_{conv}^{T} and $F_{conv}^{q_v}$. The two diffusive fluxes F_{diff}^{T} and $F_{diff}^{q_v}$ are not explicitly available but have to be calculated from the corresponding tendencies. The necessary formulae are assembled in Appendix B.

4.4 Numerical implementation of the flux algorithm

The right-hand sides of the relations (25), (26) are usually understood as vertical averages over model layers and considered as valid on full model levels η_x. For example, in the IFS Eq. (27) may be generalized to the vertical integral between half model levels $\eta_{1-\frac{1}{2}}$, $\eta_{1+\frac{1}{2}}$:

$$-\frac{1}{g}\int_{p(\eta_{1-\frac{1}{2}})}^{p(\eta_{1+\frac{1}{2}})}\left.\frac{\partial T}{\partial t}\right|^{turb}\mathrm{d}p = \int_{p(\eta_{1-\frac{1}{2}})}^{p(\eta_{1+\frac{1}{2}})}\frac{\partial F^{T}(p)}{\partial p}\mathrm{d}p \tag{29}$$

The integrations are carried out over pressure. Since the integrands are also functions of time t and of the horizontal coordinates λ, φ it follows:

$$-\frac{1}{g}\left.\frac{\partial T}{\partial t}\right|^{turb}\Delta p = F^{T}(t,\lambda,\varphi,\eta_{1+\frac{1}{2}}) - F^{T}(t,\lambda,\varphi,\eta_{1-\frac{1}{2}}). \tag{30}$$
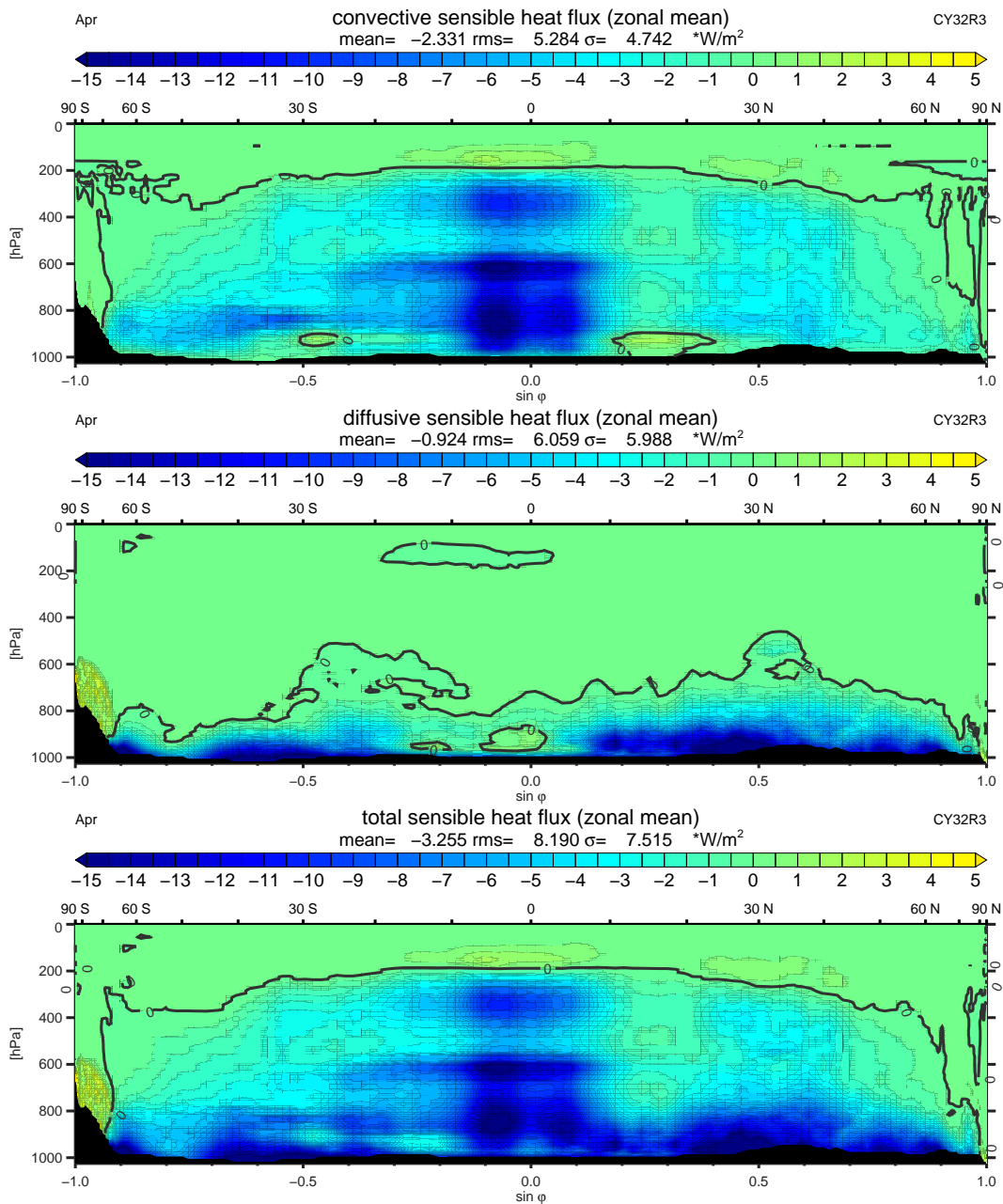
Figure 2: Zonal mean of the contributions to the sensible heat flux from convection (kinematic flux F_{conv}^T, upper picture) and diffusion scheme (kinematic flux F_{diff}^T, middle) and their sum w (lower picture) according to Eq. (28). Valid for April of the climate run.
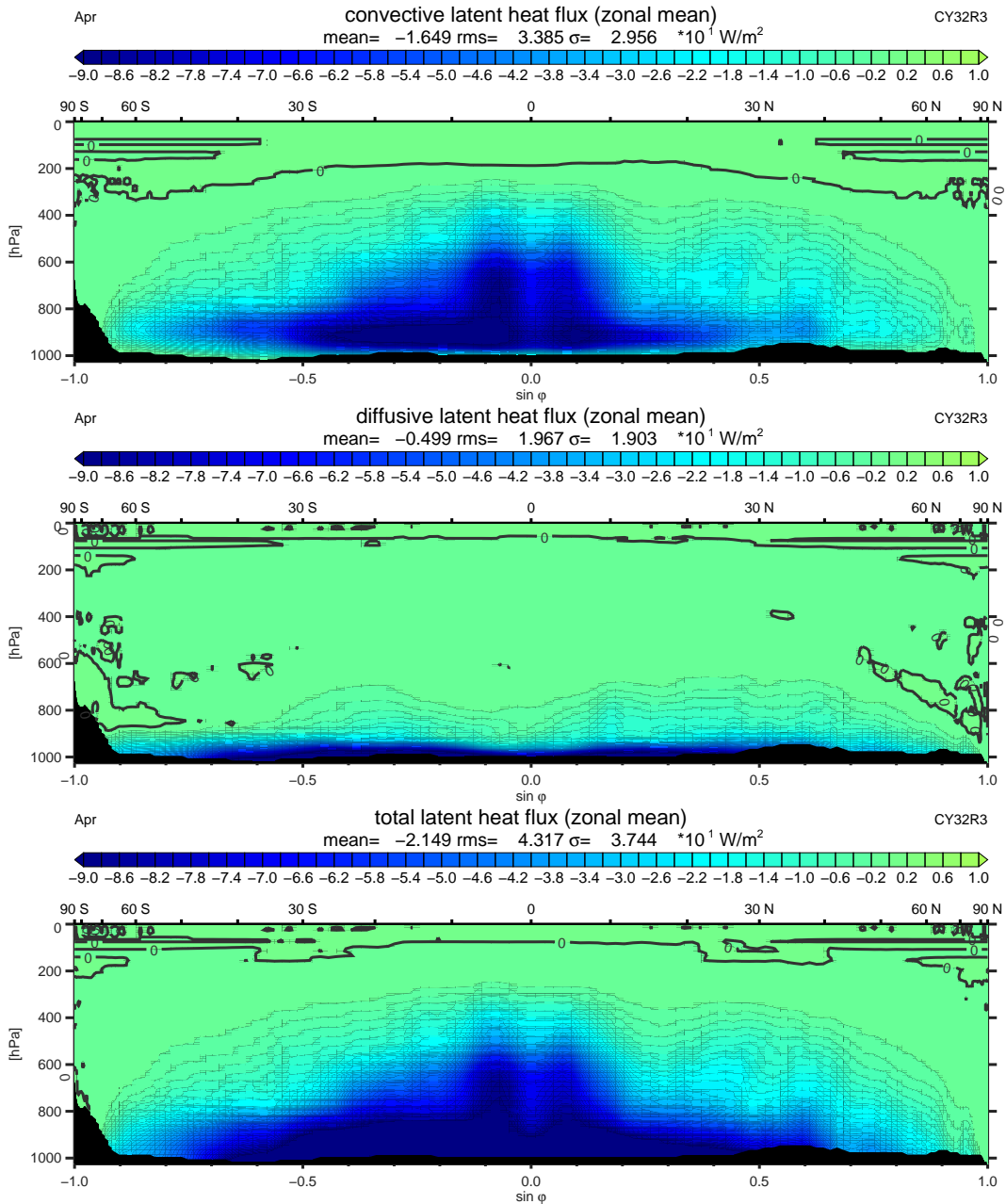
Figure 3: Zonal mean of the contributions to the latent heat flux from convection (kinematic flux $F_{conv}^{q_v}$, upper picture) and diffusion scheme (kinematic flux $F_{diff}^{q_v}$, middle) and their sum f (lower picture) according to Eq. (28). Valid for April of the climate run.

Name	Unit	Field
T	[K]	Temperature
q_v	[ ]	Specific humidity
$\langle PREC_{cloud} \rangle$	[m]	Accumulated surface large scale precipitation
$\langle PREC_{conv} \rangle$	[m]	Accumulated surface convective precipitation
$\langle SH \rangle$	[W/m^2*s]	Accumulated surface sensible heat flux
$\langle LH \rangle$	[W/m^2*s]	Accumulated surface latent heat flux

Table 1: Fields routinely stored in the IFS for every operational model run. For definition of operator $\langle \rangle$ see Eq. (31).

The left of this equation is a function of $t, \lambda, \varphi, \eta_1$; it is defined at every grid cell in the IFS. Note that Δp is generally not constant between constant half levels $\eta_{1-\frac{1}{2}}$, $\eta_{1+\frac{1}{2}}$ (neither in time nor in space). (30) yields, with boundary condition $F^T(t, \lambda, \varphi, 0) = 0$, the vertical profile of F^T at every time step and at every geographical position. It can be integrated with respect to time to yield the accumulated flux; likewise, it can be integrated horizontally with respect to λ, φ to yield the global average of F^T on the respective η-level.

4.5 Archiving temporal mean fluxes/tendencies

It is common practice at ECMWF to archive time integrated tendencies and fluxes for data evaluation from forecast runs. This is the appropriate implementation to investigate local tendencies of state variables.

However, for the evaluation of energy budgets as intended in this study it is essential to account for the temporal mass variations of the model layers; i.e. variations of Δp. This is implemented here by archiving time integrated tendencies weighted by the layer thickness Δp. Integrating (30) over time shows that only these weighted tendencies are consistent with the time integrated fluxes.

The global gridscale conversion rate $C = \{-\overline{\alpha}\,\overline{\omega}\}$ is most sensitive to mass variations. When it is calculated by time integration and following mass integration the result is 5.1 Wm^{-2}, while the accurate result from mass integration followed by time integration is 3.4 Wm^{-2}. In order to guarantee correct temporal mass means and consistency between tendencies and fluxes the present study deviates from ECMWF standard in that mass weighted tendencies were archived. Only in subsection 6.1 the standard ECMWF archiving mode was used.

5 Model Setup

In this study monthly mean parameterized tendencies/fluxes were extracted from a one year forecast run of the IFS (Cycle 32R3). The spectral resolution used was T159 corresponding to a reduced Gaussian grid with an approximate distance between gridpoints of 125 km. In the vertical 60 hybrid model layers were used. The integrations were initialized from the ERA40; they used analyzed sea surface temperatures. The annual model integrations were checked against ERA40 and surface and satellite observations. The results were in reasonable agreement; a long-term drift in the model state can be excluded. In addition to the parameterized tendencies/fluxes used to calculate w and f all tendencies necessary to reproduce the local tendencies of temperature and specific humidity using the respective budget equation were extracted from the model run.

The model fields used in this study are assembled in Tabs. 1, 2. Tab. 1 lists the fields that are routinely stored for every model run. These fields are however not sufficient for the present analysis.

Tab. 2 lists the additional fields stored within the present experiment. Accumulated weighted tendencies are

Name	Unit	Accumulated tendencies due to
$\left\langle \left.\frac{\partial T}{\partial t}\right|_{dyn} \Delta p \right\rangle$	$\left[\frac{KPa}{s}s\right]$	Dynamics including $\overline{\alpha}\,\overline{\omega}/c_p$
$\left\langle \left.\frac{\partial T}{\partial t}\right|_{\overline{\alpha}\,\overline{\omega}} \Delta p \right\rangle$	$\left[\frac{KPa}{s}s\right]$	$\overline{\alpha}\,\overline{\omega}/c_p$ separately
$\left\langle \left.\frac{\partial T}{\partial t}\right|_{diff} \Delta p \right\rangle$	$\left[\frac{KPa}{s}s\right]$	Diffusion scheme (without turbulent orographic form drag and boundary layer dissipation)
$\left\langle \left.\frac{\partial T}{\partial t}\right|_{conv} \Delta p \right\rangle$	$\left[\frac{KPa}{s}s\right]$	Convection scheme
$\left\langle \left.\frac{\partial T}{\partial t}\right|_{cloud} \Delta p \right\rangle$	$\left[\frac{KPa}{s}s\right]$	Cloud scheme
$\left\langle \left.\frac{\partial T}{\partial t}\right|_{rad} \Delta p \right\rangle$	$\left[\frac{KPa}{s}s\right]$	Radiation scheme
$\left\langle \left.\frac{\partial T}{\partial t}\right|_{remain} \Delta p \right\rangle$	$\left[\frac{KPa}{s}s\right]$	horizontal diffusion K_T, turbulent orographic form drag, boundary layer dissipation
$\left\langle \left.\frac{\partial q_v}{\partial t}\right|_{dyn} \Delta p \right\rangle$	$\left[\frac{1Pa}{s}s\right]$	Dynamics
$\left\langle \left.\frac{\partial q_v}{\partial t}\right|_{diff} \Delta p \right\rangle$	$\left[\frac{1Pa}{s}s\right]$	Diffusion scheme
$\left\langle \left.\frac{\partial q_v}{\partial t}\right|_{conv} \Delta p \right\rangle$	$\left[\frac{1Pa}{s}s\right]$	Convection scheme
$\left\langle \left.\frac{\partial q_v}{\partial t}\right|_{cloud} \Delta p \right\rangle$	$\left[\frac{1Pa}{s}s\right]$	Cloud scheme
$\left\langle \left.\frac{\partial q_{li}}{\partial t}\right|_{para} \Delta p \right\rangle$	$\left[\frac{1Pa}{s}s\right]$	Conversion to liquid/frozen water (due to entire parametrization)
$\left\langle \left.\frac{\partial q_l}{\partial t}\right|_{diff} \Delta p \right\rangle$	$\left[\frac{1Pa}{s}s\right]$	Diffusion scheme
$\left\langle \left.\frac{\partial q_i}{\partial t}\right|_{diff} \Delta p \right\rangle$	$\left[\frac{1Pa}{s}s\right]$	Diffusion scheme

Name	Unit	Accumulated fluxes due to
$\left\langle F_{conv}^T \right\rangle$	$\left[\frac{Kkg}{m^2 s}s\right]$	Turbulence (convection scheme)
$\left\langle F_{conv}^{q_v} \right\rangle$	$\left[\frac{kg}{m^2 s}s\right]$	Turbulence (convection scheme)
$\left\langle F_{conv}^{q_{li}} \right\rangle$	$\left[\frac{kg}{m^2 s}s\right]$	Turbulence (convection scheme)
$\left\langle F_{conv}^{precl} \right\rangle$	$\left[\frac{kg}{m^2 s}s\right]$	Liquid convective precipitation
$\left\langle F_{conv}^{preci} \right\rangle$	$\left[\frac{kg}{m^2 s}s\right]$	Frozen convective precipitation
$\left\langle F_{cloud}^{precl} \right\rangle$	$\left[\frac{kg}{m^2 s}s\right]$	Liquid large scale precipitation
$\left\langle F_{cloud}^{preci} \right\rangle$	$\left[\frac{kg}{m^2 s}s\right]$	Frozen large scale precipitation

Table 2: Special fields stored within the present experiment in addition to the routinely stored fields.

denoted as $\left\langle \left. \frac{\partial X}{\partial t} \right|_y \Delta p \right\rangle$, accumulated fluxes as $\left\langle F_y^X \right\rangle$. The symbol X indicates the state variable involved (temperature T, specific humidity q_v, liquid cloudwater q_l, frozen cloudwater q_i, combined liquid/frozen cloudwater q_{li}, liquid precipitation $prec\,l$ and frozen precipitation $prec\,i$), the subscript y the governing process (convection, diffusion, cloud scheme). The operator $\langle \rangle$ is defined as:

$$\langle AB \rangle = \int_{t_0}^t AB\,\mathrm{d}t. \tag{31}$$

It is a shorthand notation for the time integral from the initial time t_0 of the forecast until the time t for which the accumulated field is eventually archived. The integrand is a possible product AB of all time-dependent functions A, B involved. Note that the result $\langle AB \rangle$ remains to be a function of the upper limit t of the integration.

Tab. 2 contains, in addition to the tendencies of T and q_v, tendencies of q_l, q_i and q_{li} which are required in the calculation of the diffusive contribution to both w and f (see Appendix B). All fields of Tabs. 1, 2 were stored every 24 hours. They represent the data basis for the present study.

Mean fields for the period from time t_1 to time t_2 can now be calculated from the accumulated fields. For weighted apparent tendencies this reads for example:

$$\left. \frac{\partial T}{\partial t} \right|_{conv} \Delta p = \frac{\left\langle \left. \frac{\partial T}{\partial t} \right|_{conv} \Delta p \right\rangle (t_2) - \left\langle \left. \frac{\partial T}{\partial t} \right|_{conv} \Delta p \right\rangle (t_1)}{t_2 - t_1}. \tag{32}$$

In the same way mean fluxes are calculated, for example:

$$F_{conv}^T = \frac{\left\langle F_{conv}^T \right\rangle (t_2) - \left\langle F_{conv}^T \right\rangle (t_1)}{t_2 - t_1}. \tag{33}$$

In the course of this work experiments with various periods were carried out. However, in the present paper the focus is on monthly mean fluxes (i.e., $t_2 - t_1 = 1$ month).

6 Consistency checks

Two different consistency checks were applied on the data from the special model run. First the residuals of Eqs. (18), (19) were examined. Second the surface fluxes of w and f from Eqs. (28) were compared with the routinely stored surface fluxes (Tab. 1). Both consistency checks were carried out for the first month of the one year climate run (i.e., for 'August')

6.1 Residuals of the forecast equations

The monthly mean gridscale tendencies of temperature and specific humidity *on the left* of Eqs. (18), (19) are calculated from the routinely stored fields of $\overline{T}$ and $\overline{q}_v$ (Tab. 1). The appropriate apparent tendencies *on the right* of (18), (19) are individually very large compared with the gridscale tendencies. They were obtained from a one month model run. In this way the left and the right hand sides of Eqs. (18), (19) were independently specified. The difference between both sides is called here the *residual* of the forecast equations (18), (19).
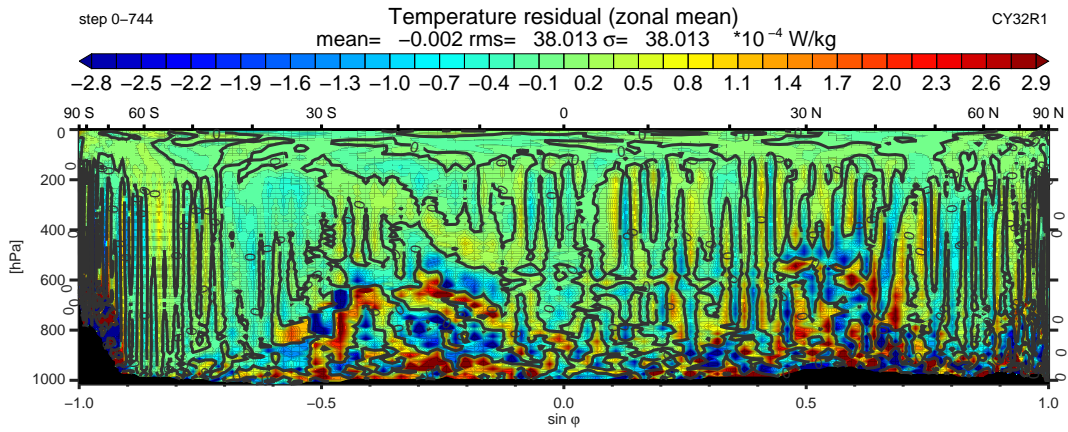
Figure 4: Zonal mean of the residual of Eq. (18). The residual is calculated from the mean tendencies of the first forecast month.
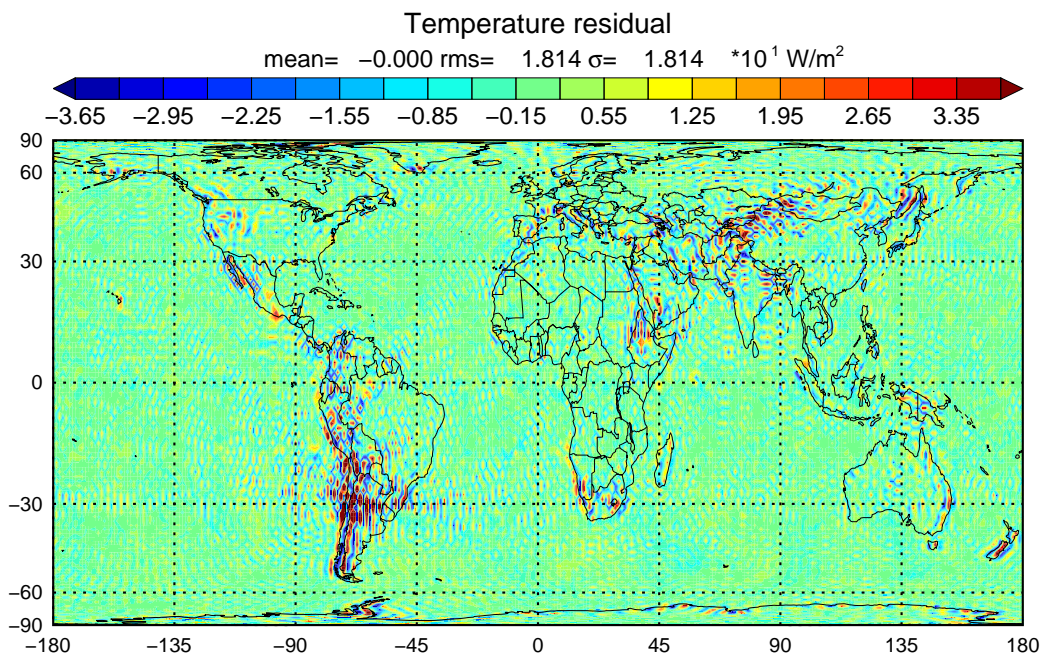
Figure 5: Vertical integral of the residual of Eq. (18). The residual is calculated from the mean tendencies of the first forecast month.

Since the residual should be zero at every single time step it is possible in this special case to exchange time and mass integration. This test was therefore not made in the mass-weighted archiving mode but in the regular ECMWF mode.

For the specific humidity (Eq. 19, no figure shown) the rms-value of the residual is three orders of magnitude smaller than the corresponding rms-value of the local tendency. The global mass mean of the residual is five orders of magnitude smaller than the mean of the local tendency. Considering the complexity of the IFS these figures are considered as satisfyingly small.

For the temperature (Eq. 18, Figs. 4, 5) the results are less satisfactory. The global mass mean of the residual is -1.55×10^{-7} W/kg, compared to the mean of the temperature tendency of -6.70×10^{-5} W/kg, corresponding to a linear mean residual of 0.2 %; this appears as acceptable. However, the rms-value of the residual is twice that of the tendency (rms of residual 3.80×10^{-3} W/kg, rms of tendency 1.78×10^{-3} W/kg).

The main reason for this strong imbalance seems to be the semi-implicit solution technique applied in the local temperature forecast equation. The purpose of this technique is to filter fast gravity waves; these are generated predominantly in mountainous terrain. This explains why the residual discrepancy of the temperature forecast equation found in Fig. 5 is most pronounced over the Andes and the Himalayas.

The semi-implicit effect cannot be extracted for specific gridpoints; further, it cannot be split into a gridscale and a sub-gridscale fraction. For these reasons, the residual was considered as additional apparent temperature tendency generated by the gridscale dynamics and consequently lumped into $\partial T / \partial t |_{dyn}$.

6.2 Residuals of the surface fluxes

The consistency of the turbulent fluxes calculated from Eqs. (28) is tested by comparing them with the operationally stored surface fluxes of sensible and latent heat from the surface parametrization. Figs. 6, 7 show the difference between the operationally stored surface fluxes and the calculated surface fluxes w and f, respectively. The global rms-mean of the difference is about 2 % of the parameterized flux in the case of w and about 0.1 % in the case of f. The strongest differences in Fig. 6, typically of the order 5 W/m^2, are found in a few regions limited to high orography. Concerning the negative anomalies over the subtropical southern oceans in Fig. 7 note that these discrepancies are typically below 0.3 W/m^2. For these reasons the overall imbalance in Figs. 6, 7 can be considered satisfyingly small.

7 Results

The local gridscale conversion rate $-\overline{\alpha}\,\overline{\omega}$, contained in the budget equation of temperature, was calculated at every time step in the model run and stored as accumulated mass-weighted tendency. The local sub-gridscale conversion rate $-\overline{\alpha' \omega'}$ was calculated from Eq. (9) using the fluxes w and f. Also, the gridscale efficiency factor $\overline{N}$ and the response $\overline{R}$ of the atmosphere to heating (i.e., both the gridscale and sub-gridscale components $\overline{R}^{grid}$, $\overline{R}^{sub}$) were calculated. With these fields the conversion rate and the generation rate of the Lorenz cycle, both in its gridscale and sub-gridscale components, were estimated. The global patterns of these quantities will be discussed first, followed by the corresponding global means.

SH−ws (Aug)

mean= −0.087 rms= 0.580 σ= 0.573 *W/m^2

−5.0 −4.2 −3.4 −2.6 −1.8 −1.0 −0.2 0.6 1.4 2.2 3.0 3.8 4.6
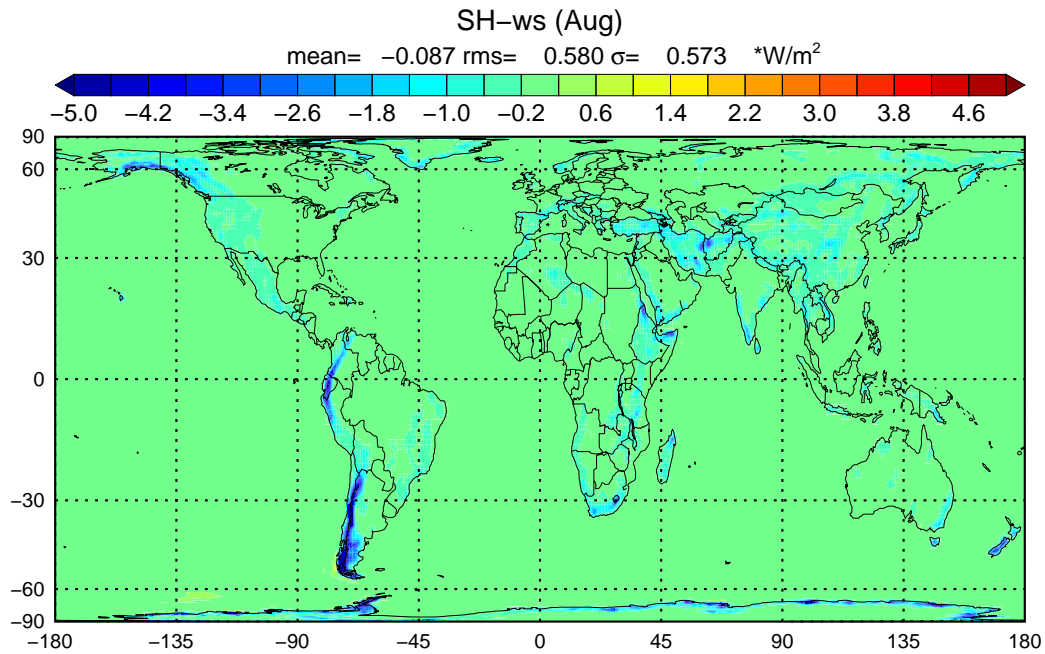
Figure 6: *Difference of routinely stored surface sensible heat flux and surface sensible heat flux calculated from Eqs. (28).*

LH−fs (Aug)

mean= −0.708 rms= 1.389 σ= 1.195 *10^{-1} W/m^2

−3.1 −2.8 −2.5 −2.2 −1.9 −1.6 −1.3 −1.0 −0.7 −0.4 −0.1 0.2 0.5 0.8 1.1 1.4 1.7
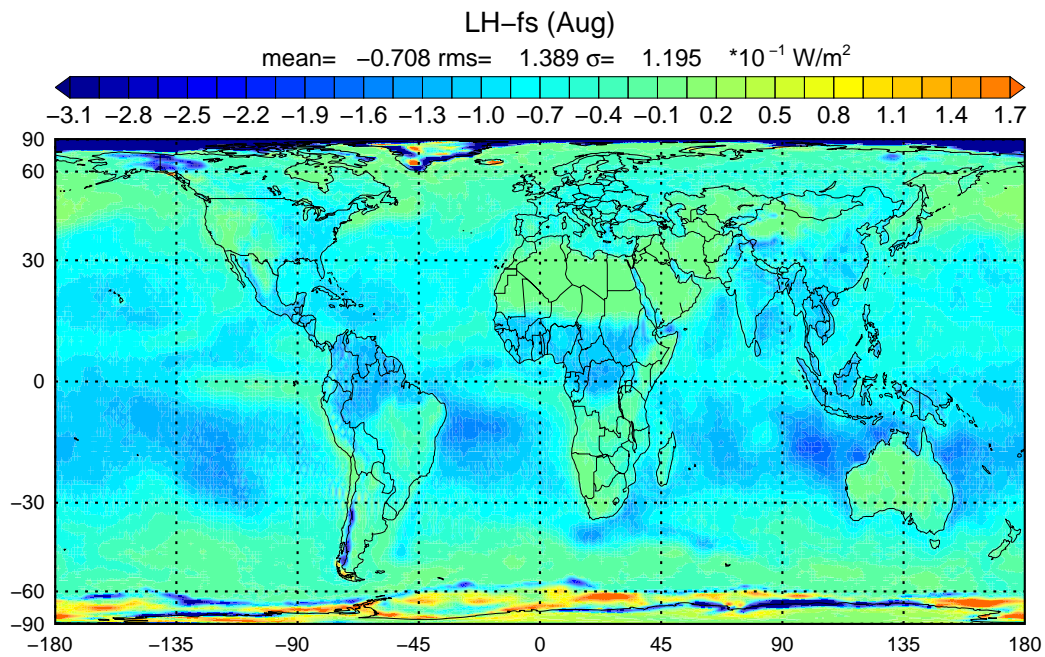
Figure 7: *Difference of routinely stored surface latent heat flux and surface latent heat flux calculated from Eqs. (28).*
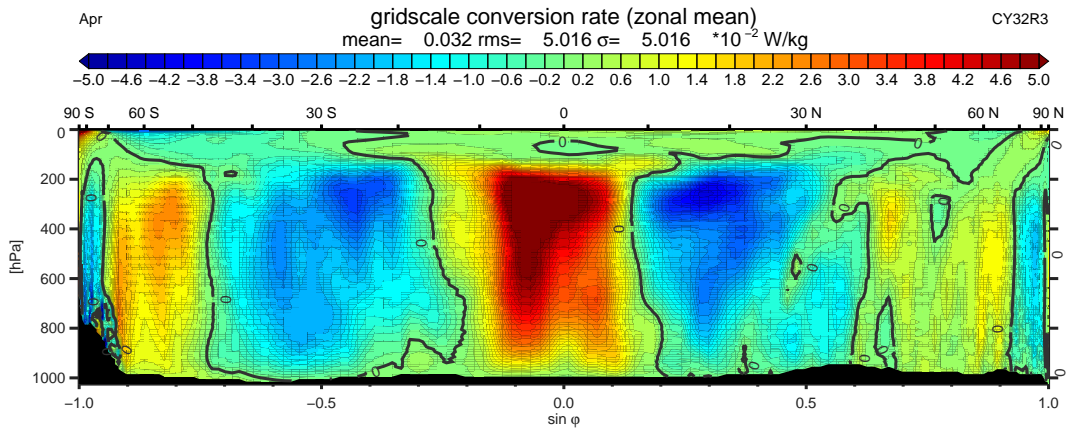
Figure 8: *Zonal mean of the local gridscale conversion rate* $-\overline{\alpha}\,\overline{\omega}$, *valid for the month April of the climate run.*
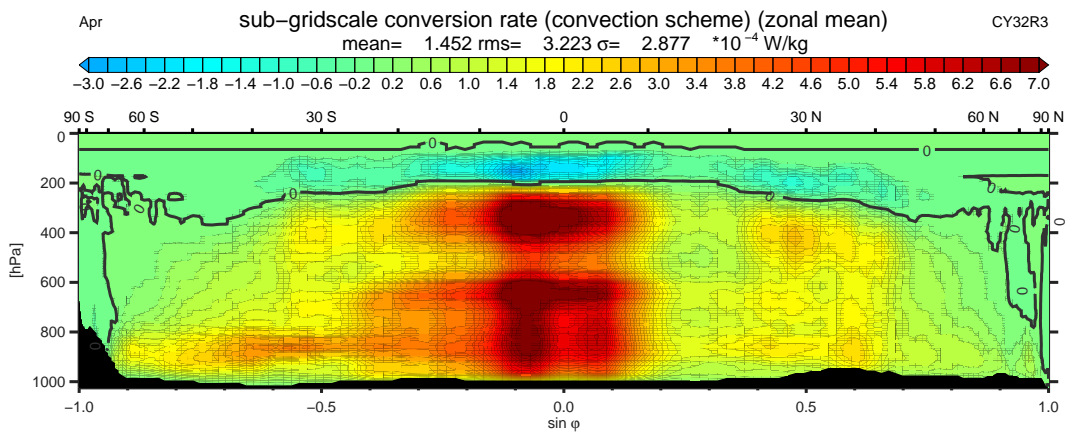
Figure 9: *Zonal mean of the local sub-gridscale conversion rate* $-\overline{\alpha'\omega'}$, *calculated from fluxes w and f extracted exclusively from the convection scheme. Valid for the month April of the climate run.*
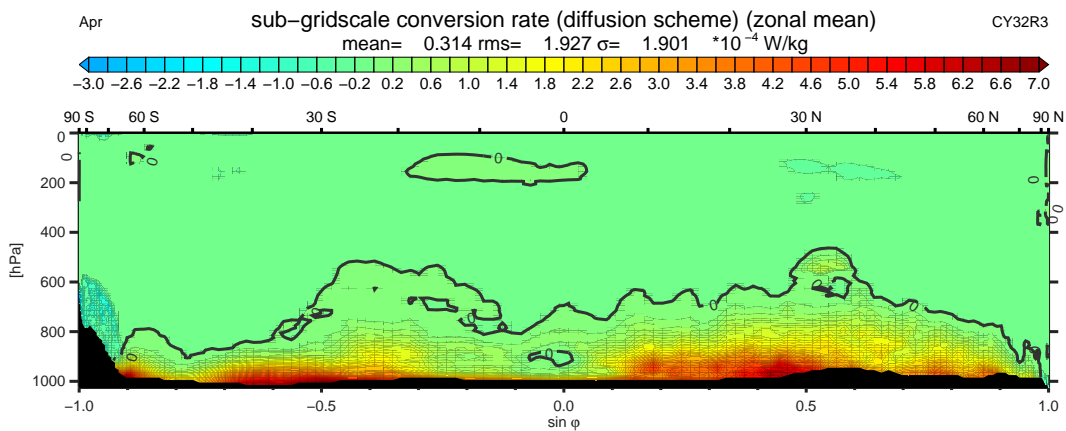
Figure 10: *Like Fig. 9, but extracted exclusively from the diffusion scheme.*

gridscale conversion rate (Apr)
mean= 0.032 rms= 3.704 σ= 3.703 *10^2 W/m^2
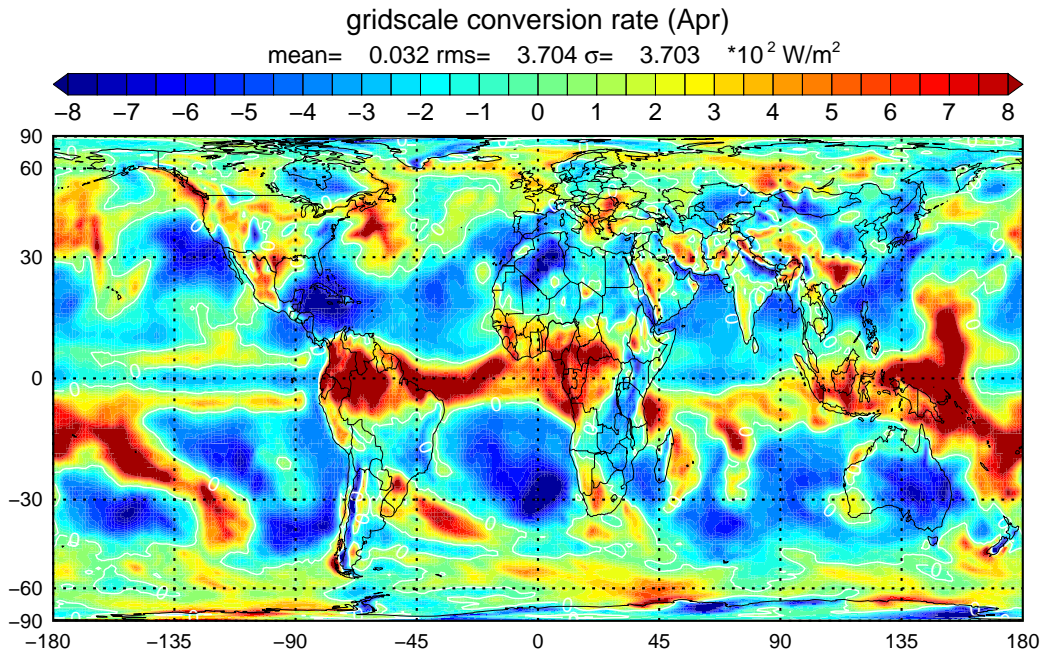
Figure 11: Vertical mean of the local gridscale conversion rate $-\overline{\alpha}\,\overline{\omega}$, valid for the month April of the climate run. Same as Fig. 8 but vertical integral instead of zonal mean.

sub−gridscale conversion rate (Apr)
mean= 1.775 rms= 2.720 σ= 2.060 *W/m^2
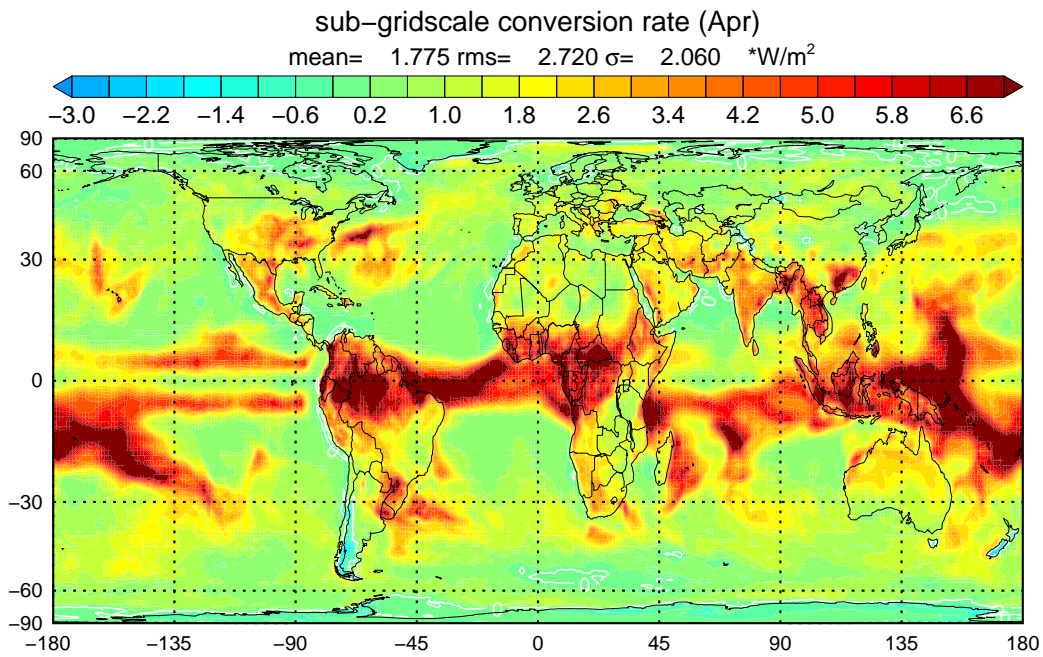
Figure 12: Vertical mean of the local sub-gridscale conversion rate $-\overline{\alpha'\omega'}$, calculated from fluxes w and f. Valid for the month April of the climate run. Same as Fig. 11 but for buoyancy flux instead of $-\overline{\alpha}\,\overline{\omega}$.
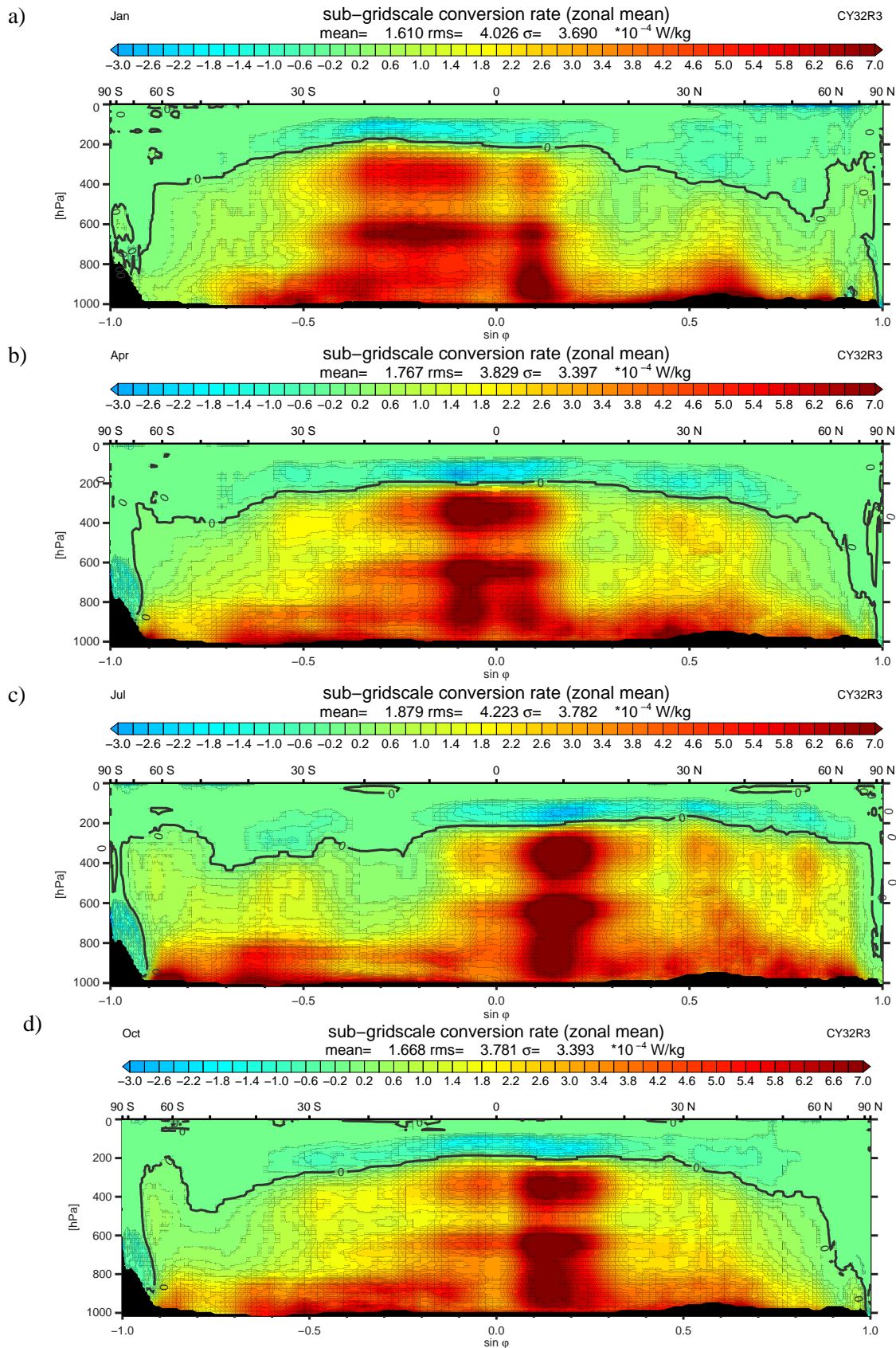
Figure 13: *Zonal mean of the local sub-gridscale conversion rate* $-\overline{\alpha'\omega'}$, *calculated from fluxes w and f. Valid for the months January, April, July and October of the climate run. Second individual plot (April) equal to sum of Figs. 9, 10.*

7.1   Global patterns of the local conversion rates

Fig. 8 displays, for one selected month (April) of the one year climate run, the zonal mean global distribution of the local gridscale conversion rate $-\overline{\alpha}\,\overline{\omega}$. This quantity is a strong component of the sensible heat budget of the atmosphere (e.g., HH-I or Hamelbeck et al., 2001). The global rms-value of the corresponding sub-gridscale quantity in Fig. 9, the buoyancy flux $-\overline{\alpha'\omega'}$, is typically two orders of magnitude smaller. Fig. 9 has been calculated with data exclusively from the convection scheme.

The contribution of small scale turbulence to the buoyancy flux, parameterized by the diffusion scheme of the IFS, is plotted in Fig. 10 for the same month. The global mean, both linear and rms, is considerably smaller than the deep convection component of Fig. 9. Fig. 10 shows that the scheme concentrates the diffusive component of $-\overline{\alpha'\omega'}$ to the planetary boundary layer.

Thus the full buoyancy flux, i.e., the sum of Figs. 9, 10 (see Fig. 13b), is almost identical to Fig. 9. It is predominantly deep organized convection, maximum in the tropical atmosphere, that controls the conversion from sub-gridscale available potential energy into sub-gridscale kinetic energy. This is an important result. It implies that the turbulent processes in the planetary boundary layer control just a small fraction of this conversion, in naive agreement with the limited geometrical extension of the PBL.

The gridscale conversion rate, i.e., the linear global mean of Fig. 8, is about 3.2×10^{-4}W/kg; the sub-gridscale conversion rate, i.e., the linear global mean of Fig. 13b, is 1.8×10^{-4}W/kg. This shows that both gridscale and sub-gridscale processes contribute about equally to the global energy conversion rate. However, the rms-values of both global patterns are completely different: 502×10^{-4}W/kg in Fig. 8 and 3.8×10^{-4}W/kg in Fig. 13b. It shows that the gridscale conversion rate is the residual of very large values of the adiabatic term with opposite sign which almost exactly compensate each other. For the sub-gridscale conversion rate this is quite different. The rms-value of Fig. 13b is of about same magnitude as the linear global mean; this implies that the individual field value of the buoyancy flux is representative for the sub-gridscale conversion rate.

The geographical distribution of the vertical integrals of these fields are shown in Figs. 11 and 12. Both gridscale and sub-gridscale local conversion rates show distinct maxima in the ITCZ. Again it should be stressed that the global mean of both fields is of comparable size, while the fields are very different. The local gridscale conversion rate is much bigger in magnitude than the local sub-gridscale conversion rate; however, positive and negative contributions to the global mean almost cancel each other. In contrast the local sub-gridscale conversion rate is nearly everywhere positive around the globe which yields a comparable mean for much smaller individual values.

The conspicuous correlation of positive areas of $-\overline{\alpha}\,\overline{\omega}$ (Fig. 11) with maxima of $-\overline{\alpha'\omega'}$ (Fig. 12) in the tropics deserves a comment. Positive values of the gridscale adiabatic term are due to upward $\overline{\omega}$ which tends to support convection and thus should be correlated with upward buoyancy flux. However, over areas with downward $\overline{\omega}$ the buoyancy flux, while weaker, is yet upward directed. Regional examples include the equatorial band of weak but positive buoyancy flux in the Pacific and Indian Oceans or the areas with downward $\overline{\omega}$ and positive buoyancy flux over the Gulf Stream and the Kuroshio regions. Conversely, the various strong upward $\overline{\omega}$ maxima in the high latitudes (Central Siberia, coast of Antarctica) are not at all correlated with any buoyancy flux maximum.

The next step is to discuss the global distribution of the local sub-gridscale conversion rate. Its seasonal variations are presented in Fig. 13. In this plot the zonal mean of the buoyancy flux is shown for the central month of each season. The figure shows, throughout the global atmosphere and throughout the year, the general upward directed buoyancy flux. One of the three requiremens of a rational, well posed, and physically reasonable, parametrization scheme, postulated by Arakawa (2004), is that the parametrization '*should be based on the concept of buoyancy*'. According to Arakawa, '*this is a physically reasonable requirement since cumulus convection is buoyant convection, which recognizes its environment primarily through the buoyancy force*'. Fig.

13 demonstrates that this requirement has indeed been fulfilled by the present IFS run. The buoyancy flux, implicitly contained in the model forecast run, is maximum throughout the year in the ITCZ. It reaches up to the tropopause which throughout the atmosphere is recognizeable as the zero line of $-\overline{\alpha'\omega'}$.

The buoyancy flux is at its maximum in northern summer, when convection over the land areas of the northern hemisphere peaks. A corresponding peak on the southern hemisphere does not exist due to the dominating influence of the ocean area.

7.2 Global patterns of the local generation rates

In order to estimate the generation rate G^{grid} the global distribution of $\overline{R}$ is needed. This quantity, introduced as the *response* in HH-II, has been defined in Eq. (11). The zonal mean of the gridscale response $\overline{R}$, as extracted from the IFS, is plotted in Fig. 14.

This quantity was originally evaluated by Hantel and Baader (1978); their data set (adopted from Oort and Rasmusson, 1971) was limited to coarse gridscale data 1958-1963 of the northern hemisphere, (see also Fig. 9.10 in Gill, 1982). The same quantity was evaluated for the seasons 1979-1989 with ECMWF data (see pages 132, 136, 140, 144 of Hoskins et al., 1989) and again by Fortelius (1995).

Fig. 14 is in quite good agreement with these earlier evaluations. For example, the global field of $\overline{R}$ reproduces the climatic zones: Condensational heating dominates in the ITCZ and in midlatitude storm tracks; radiational cooling dominates in the cloud free latitudes of the subtropics and over the polar caps. Specific details, beyond the scope of the present study, are visible in the field of $\overline{R}$ in its annual course. For example, the positive area of $\overline{R}$ around 600 hPa in the extratropics is well separated from the boundary layer; it is caused by the precipitation generating processes in these latitudes. Another example is the boundary layer heating as well as the stratospheric layer heating.

The innovative aspect in Fig. 14 is however the fact that the sub-gridscale component has now become accessible and is fully included in $\overline{R}$. For example, Hantel and Baader (1978) were forced to lump the *subsynoptic term*, as they called it, into the quantity Q, because they had no possibility to estimate $\overline{R}^{sub}$. The sub-gridscale contribution to the present $\overline{R}$ is by no means negligible; it constitutes the second part of $\overline{R}$ according to Eq. (11). The structure of the global field of $\overline{R}^{sub}$ (not shown) is dominated by the vertical divergence of the turbulent sensible heat flux; the buoyancy flux, the second part of $\overline{R}^{sub}$, is practically not visible. However, the global mean of the turbulent sensible heat flux divergence is zero, since the turbulent sensible heat flux vanishes at the surface and at top of the atmosphere (note: the molecular sensible heat flux, only effective in the skin layer of the surface is not included in Eq. 11). Conversely, the buoyancy flux has a global average of 1.73 W/m^2.

The efficiency factor, defined in Eq. (5) and indispensable for estimating the generation rate of available potential energy, has been calculated from the reference pressure; p_r was obtained as the average of p on isentropic surfaces. The corresponding gridscale $\overline{N}$ is plotted in Fig. 15. It is broadly correlated with the pattern of $\overline{R}$. To what extent it is advisable to search for a sub-gridscale efficiency factor in order to evaluate $\overline{N'Q'}$ and its corresponding global integral G^{sub} may be left here for later consideration.

7.3 A new estimate of the Lorenz global energy cycle

The local and global quantities discussed in this study, which are required for a state-of-the-art estimate of the classical Lorenz energy cycle, complete with the sub-gridscale components, are listed in Tab. 3. All quantities in this table have been explicitly evaluated from the results of the present one year IFS run in climate mode *except the sub-gridscale generation rate $\overline{N'R'}$ and its corresponding global average G^{sub}*. The global patterns

a)

b)

c)

d)
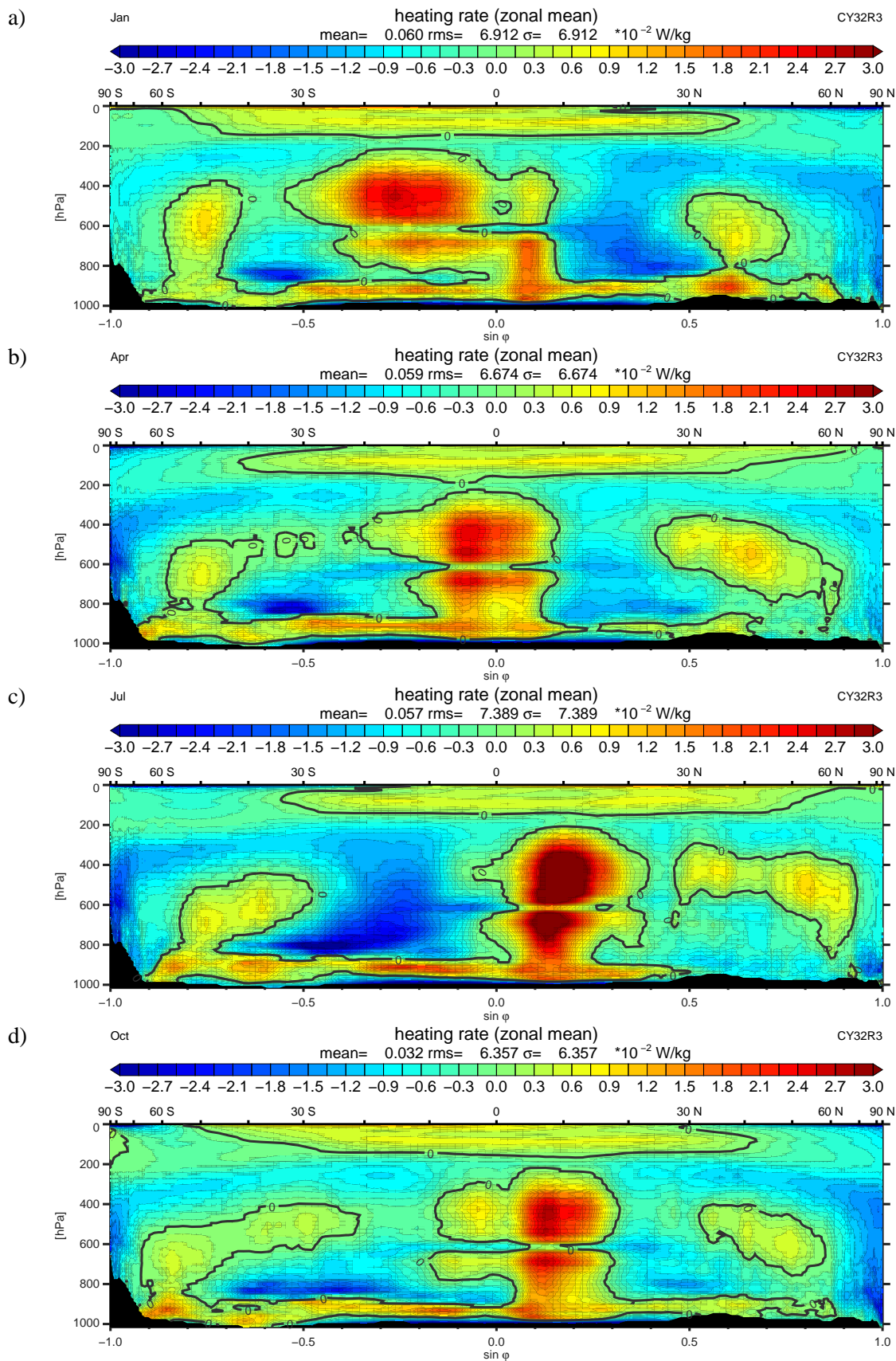
Figure 14: Zonal mean of $\overline{R}$. Valid for the months January, April, July and October of the climate run.
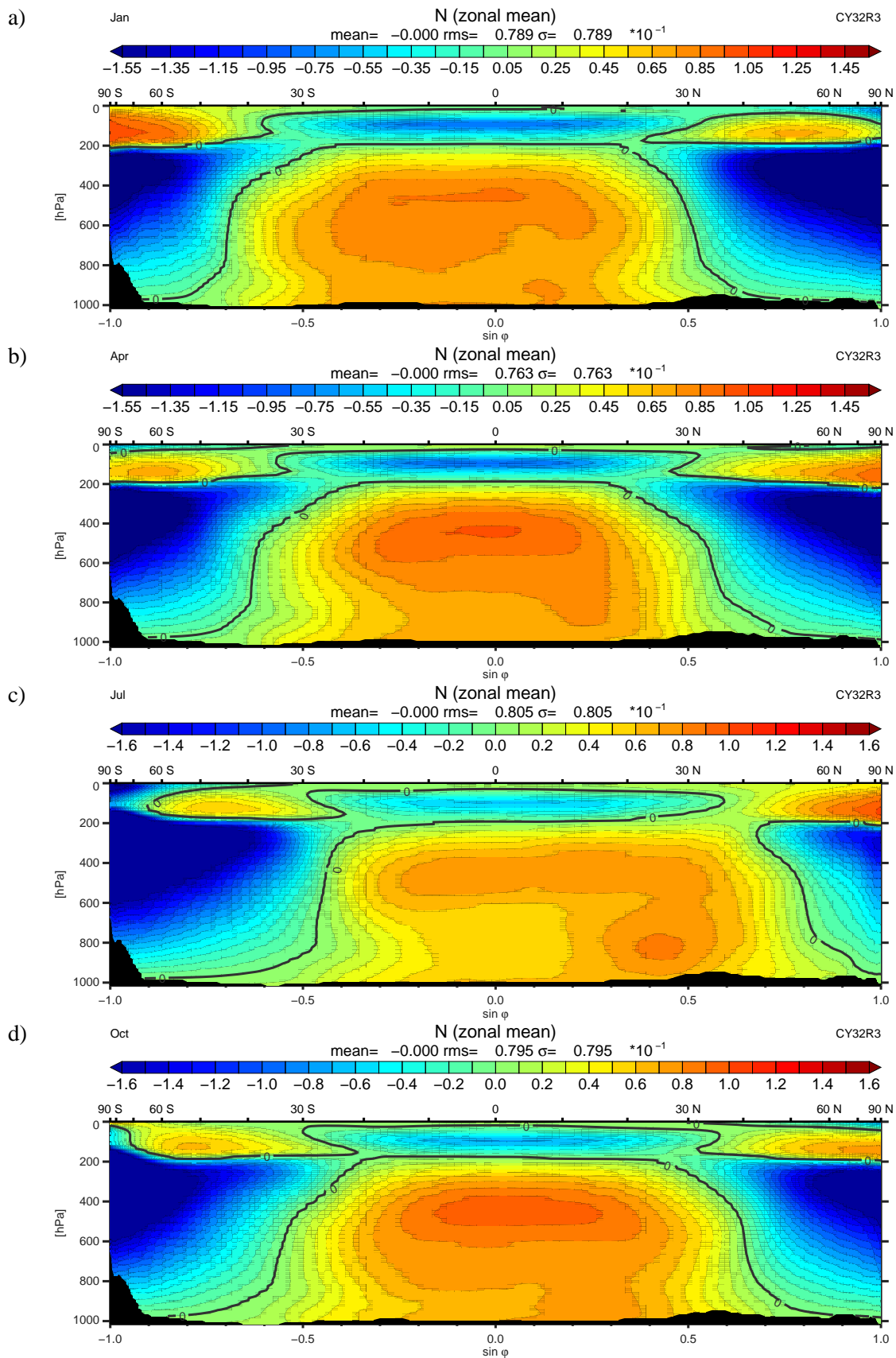
Figure 15: Zonal mean of the efficiency factor $\overline{N}$. Valid for the months January, April, July and October of the climate run.
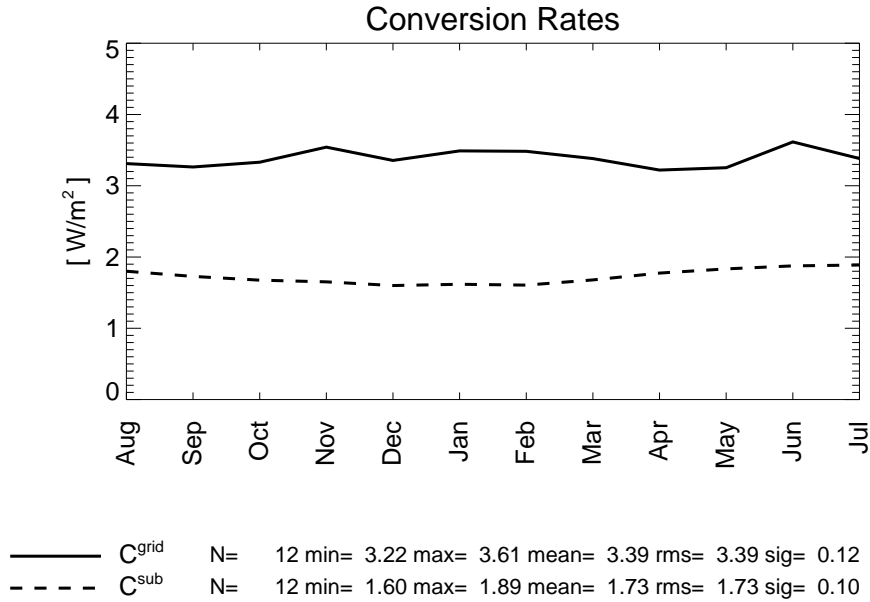
Figure 16: Time series of monthly mean gridscale and sub-gridscale conversion rates calculated from the one year climate forecast.
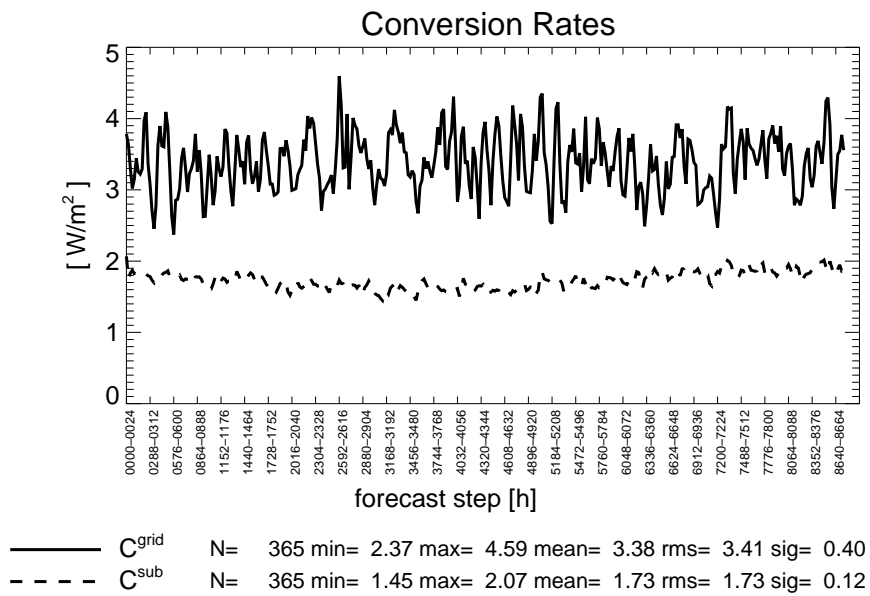
Figure 17: Time series of 24 hourly gridscale and sub-gridscale conversion rates calculated from the one year climate forecast.

Generation Rates

		N=	min=	max=	mean=	rms=	sig=
——	G^{grid}_{day}	365	2.15	4.04	3.20	3.22	0.29
- - - -	G^{grid}_{month}	12	2.71	3.21	3.00	3.00	0.16
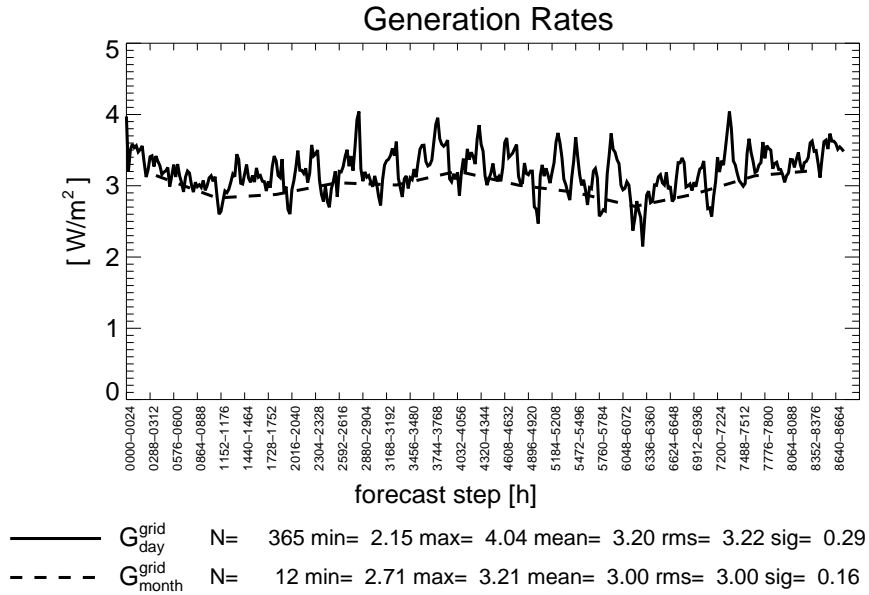
Figure 18: Time series of 24 hourly (full curve) and monthly (dashed curve) gridscale generation rate, calculated from the one year climate forecast.

Heating Rates

		N=	min=	max=	mean=	rms=	sig=
——	$\overline{R}$	12	2.45	9.07	5.38	5.68	1.89
- - - -	$\overline{R}^{grid}$	12	0.72	7.19	3.66	4.07	1.87
··········	$\overline{R}^{sub}$	12	1.60	1.89	1.73	1.73	0.10
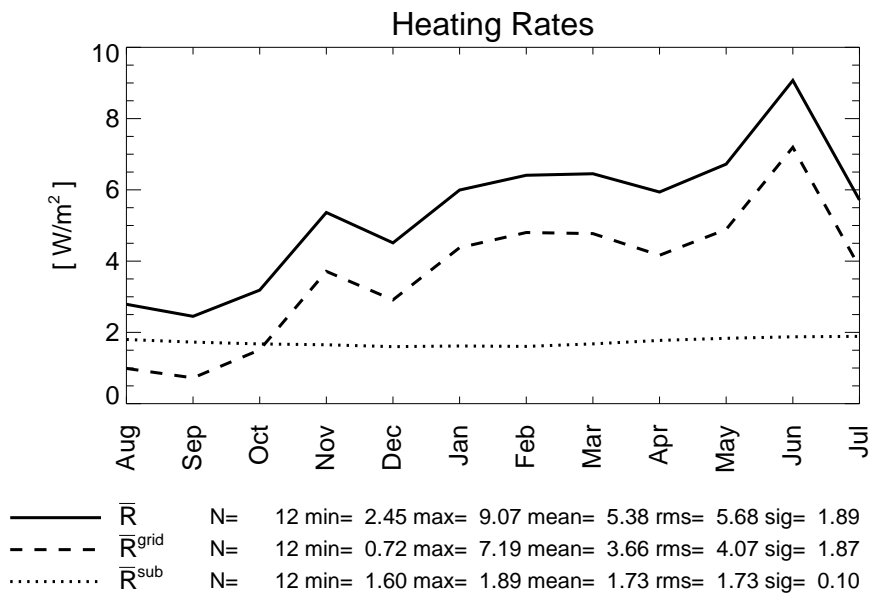
Figure 19: Time series of monthly mean gridscale and sub-gridscale heating rates calculated from the one year climate forecast.

	local	global
HEATING RATE		
total	$\overline{R}$	$\{\overline{R}\}$
gridscale	$\overline{R}^{grid}$	$\{\overline{R}^{grid}\}$
sub-gridscale	$\overline{R}^{sub}$	$\{\overline{R}^{sub}\}$
GENERATION RATE		
total	$\overline{NR}$	$G = \{\overline{NR}\}$
gridscale	$\overline{N}\,\overline{R}$	$G^{grid} = \{\overline{N}\,\overline{R}\}$
sub-gridscale	$\overline{N'R'}$	$G^{sub} = \{\overline{N'R'}\}$
CONVERSION RATE		
total	$-\overline{\alpha\omega}$	$C = \{-\overline{\alpha\omega}\}$
gridscale	$-\overline{\alpha}\,\overline{\omega}$	$C^{grid} = \{-\overline{\alpha}\,\overline{\omega}\}$
sub-gridscale	$-\overline{\alpha'\omega'}$	$C^{sub} = \{-\overline{\alpha'\omega'}\}$

Table 3: Heating-, generation and conversion rates relevant for the global Lorenz energy cycle and discussed in this study, stratified into local and global quantities and gridscale and sub-gridscale contributions.

of the column in Tab. 3 referred to as 'local' have been discussed before. The next step is to discuss the 'global' quantities which are obtained from the corresponding local quantities through global mass integration. These global quantities represent the components of a new estimate of the Lorenz energy cycle.

Time series of the monthly global mean values of gridscale and sub-gridscale conversion rates $\{-\overline{\alpha}\,\overline{\omega}\}$, $\{-\overline{\alpha'\omega'}\}$ are shown in Fig. 16. Both conversion rates show little time variation throughout the year. The slightly smaller sub-gridscale conversion rate in southern summer is in agreement with the smaller convective activity during this season; it is caused by the different land-sea distribution on the southern as opposed to the northern hemisphere.

The conversion rates C^{grid} and C^{sub} have been calculated as annual mean from the twelve monthly averages. The result is:
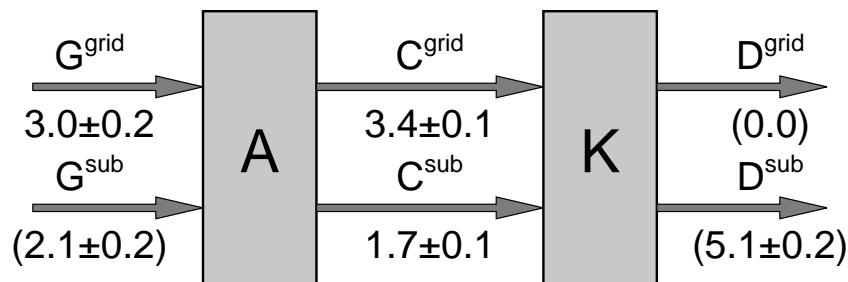
Figure 20: Global energy cycle extracted from a one year climate forecast of IFS. Reservoirs of available potential and kinetic energy A and K. Traditional gridscale conversion rates G^{grid}, C^{grid} and D^{grid}. Sub-gridscale conversion rates G^{sub}, C^{sub} and D^{sub}. Values in parentheses inferred for stationary reservoirs A and K.

$$C^{grid} = (3.39 \pm 0.12)\,\text{W/m}^2; \tag{34}$$

$$C^{sub} = (1.73 \pm 0.10)\,\text{W/m}^2; \tag{35}$$

$$C = (5.12 \pm 0.22)\,\text{W/m}^2. \tag{36}$$

The standard deviation of the monthly values in Fig. 16 has been taken as the error estimate. These figures represent the central result of the present study.

In order to study the role of the short synoptic fluctuations global averages on a daily basis have additionally been calculated. The results, corresponding to the monthly time series of Fig. 16, are plotted as daily time series in Fig. 17. The daily fluctuations of C^{grid} are 3-4 times larger than the monthly fluctuations as shown by the values of σ. However, the annual mean is practically the same in Figs. 16, 17.

This coincidence is no independent test since the monthly data have been gained by straight time integration of the daily data. The coincidence is predominantly a further consistency check of the present numerical experiment. However, it also adds additional daily variance. The first main message from Figs. 16, 17 is that the conversion rate is relatively steady throughout the model year; one arbitrary month would already be sufficient to estimate the climate mean of both C^{grid}, C^{sub}. The second main message is the coincidence with the preliminary results of HH-II (see also Fig. 1). Their estimate $((4.7 \pm 1.7)\,\text{W/m}^2)$ coincides, within error margins, with the estimate (36).

Turning now to the gridscale generation rate G^{grid} a first estimate comes from the monthly averages of both $\overline{N}$ and $\overline{R}$ (Fig. 18, dashed curve). A second estimate is from the daily values of the same quantities (full curve). The corresponding annual means are:

$$G^{grid}_{month} = (3.00 \pm 0.16)\,\text{W/m}^2; \;\; G^{grid}_{day} = (3.20 \pm 0.29)\,\text{W/m}^2. \tag{37}$$

The errors given are from the monthly variance (the daily variance in case of G^{grid}_{day}) and thus are mostly due to the annual wave which is an overestimate. Thus the difference between the two estimates of G^{grid} is presumably significant. The difference is due to the fact that the daily efficiency factor calculated for G^{grid}_{day} caused some additional correlation with the local heating rate. This augmentation of G^{grid} should however not be interpreted as the unavailable sub-gridscale quantity G^{sub}. Rather, the figure most consistent with the other fluxes of this study appears to be G^{grid}_{month}; this estimate has been entered in Fig. 20.

Although the sub-gridscale quantity G^{sub} is unavailable, because explicit sub-gridscale data are fundamentally missing, there is an indirect way to estimate G^{sub}, by using the correspondence:

$$G^{grid} + G^{sub} = C^{grid} + C^{sub} \tag{38}$$

which should prevail in a stationary climate. From Eq. (38) together with (37) the indirect estimate of the sub-gridscale generation rate follows:

$$G^{sub} = (2.1 \pm 0.2)\,\text{W/m}^2. \tag{39}$$

This indirect estimate is the best one can presently offer. This is supported by the very small annual time

tendency of the reservoirs of both gridscale available potential and kinetic energy (not shown here) which are below 0.1 W/m^2.

There is a further, partially independent, estimate of the total generation rate in form of $\{\overline{R}\}$. This is shown in Fig. 19. The global mean of $\overline{R}^{grid}$ undergoes a considerable seasonal fluctuation with an annual mean of 3.66 W/m^2. In contrast, the global mean of $\overline{R}^{sub}$, which is identical to the one of the buoyancy flux (Eq. 11), is practically constant throughout the year with a global average of 1.73 W/m^2.

One important aspect of $\overline{R}$ is that its global mean, $\{\overline{R}\}$=5.39 W/m^2 from Fig. 19, can be taken as independent estimate of the generation rate G of available potential energy, at least in the climate time mean. The independence is of a principal nature; actually, the estimate is not independent. Since G cannot in practice be determined without reference to the sensible heat budget, which has already been the basis of $\overline{R}$, the values found for G and $\{\overline{R}\}$ are practically related to each other.

From Fig. 19, by using the sum of $\overline{R}^{grid}$ and $\overline{R}^{sub}$, it follows:

$$\{\overline{R}\} = (5.39 \pm 1.87)\,\text{W/m}^2. \tag{40}$$

The high error is due to the sizeable annual fluctuation of the heating rate seen in Fig. 19, and therefore presumably an overestimate.

It is nevertheless both important and satisfying that the estimate (36) for the Lorenz conversion rate C and the estimate (40) for the global heating rate coincide within error margins.

The results discussed are summarized in Fig. 20 which is the equivalent to Fig. 1. It represents Lorenz's global energy cycle, complete with both gridscale and sub-gridscale components, estimated from the gridscale model output and the parameterizations drawn from the IFS run, one year in climate mode. The estimates have been rounded to one decimal. Values in parentheses are the indirectly inferred estimates.

Both block figures 1 and 20 are surprisingly similar despite the fact that they are based upon entirely different and independent data sets: The estimate of HH-II upon three selected months of the preliminary ERA data set, the present estimate upon a one year forecast with the latest version of IFS. Yet the figures differ only within error margins. Therefore, this study supports the conclusion of HH-II that the sub-gridscale processes play an important role in Lorenz's global energy cycle and must be included in its evaluation.

8 Conclusions

This study has tried to estimate the convective component of the global Lorenz energy cycle with the complete data set available from a one-year run in climate mode of the ECMWF model (CY32R3). This setting offered a basic data set with unprecedented completeness and accuracy. For the purpose of completing the Lorenz energy cycle the following chain of (both theoretical and practical) tasks had to be carried out and numerically implemented:

- The equations of the global energy cycle have been written in a local form that is compatible with the Lorenz theory.

- To represent the local equations numerically on the computer requires specification of a grid. The gridscale fixes the space/time scale characteristic for the actual experiment carried out in this study with the IFS.

- Discretizing the local equations is equivalent to averaging the Lorenz energy equations over the grid cell. This process is denoted by the overbar operator. It means an average over a space/time cell the size of which is that of the IFS. Averaging nonlinear quantities in the equations generates both gridscale and sub-gridscale terms.

- Most prominent nonlinear term to be averaged is $-\alpha\omega$ in the temperature equation. Its gridscale component, explicitly included in the IFS, has been $-\overline{\alpha}\,\overline{\omega}$. Its sub-gridscale (or simply convective) component has been the buoyancy flux $-\overline{\alpha'\omega'}$. Both have been familiarly interpreted as local conversion terms between available potential and kinetic energy.

- Likewise the averaged equations involve the local generation of available potential energy, expressed as gridscale component $\overline{N}\,\overline{Q}$ and sub-gridscale component $\overline{N'Q'}$; here, N is the Lorenz efficiency factor and Q the net heating. Instead of diagnosing Q the response R of the atmosphere to Q, expressed through the sensible heat equation, has been used for diagnosing the net heating.

- Thus the following gridscale fields were directly extracted from the IFS: $\overline{\alpha}$, $\overline{\omega}$, $\overline{R}^{grid}$. The gridscale $\overline{N}$ was gained from the mean temperature and pressure fields through global averaging of p on isentropic surfaces.

- Further, the following sub-gridscale fields were indirectly computed from the IFS: The buoyancy flux $-\overline{\alpha'\omega'}$ was gained through determining the sensible and latent heat fluxes f and w and using Eq. (9). The sub-gridscale $\overline{R}^{sub}$ was gained from w and $-\overline{\alpha'\omega'}$ by using Eq. (11). The correlation $\overline{N'Q'}$ could not be estimated.

- From these local quantities the corresponding generation and conversion rates G^{grid}, C^{grid}, C^{sub} were gained through global mass integration.

- G^{sub} could not be determined. However, since in the climate mean G should be equal to C the sub-gridscale generation rate was estimated indirectly from G^{grid}, C^{grid}, C^{sub}.

With these steps the goal of independently estimating the key components of the global energy cycle in form of Fig. 20 has been reached. The most important results have been as follows:

- The buoyancy flux is directed upward throughout most of the global atmosphere; it is largely controlled by the mechanism of deep convection and thus has its maxima in the tropics. This corroborates the results first reported in HH-II that the buoyancy flux represents the integrand of the new sub-gridscale conversion rate C^{sub} from available potential to kinetic energy. C^{sub} is to be considered as a relevant component of the global energy cycle.

- The gridscale conversion rate C^{grid} from available potential to kinetic energy has come out somewhat larger as the earlier estimates.

- The same is valid of the gridscale generation rate G^{grid} of available potential energy.

- The new sub-gridscale generation rate G^{sub} of available potential energy could not be independently estimated but was found from balance requirements.

- By including the sub-gridscale components the Lorenz energy cycle from the one-year climate run of the IFS has been completely determined and is reproduced in Fig. 20.

- According to Fig. 20 the intensity of the global atmospheric circulation is $(5.1 \pm 0.2)\,\mathrm{W/m^2}$. This is about twice as intense as all existing earlier estimates have suggested (e.g., Li et al., 2007).

apparent tendency		turbulent transport		condensation/ sublimation		freezing		dissipation		gravity wave drag
$\left.\frac{\partial T}{\partial t}\right|_{diff}$	$=$	$\left.\frac{\partial T}{\partial t}\right|_{diff}^{turb}$	$+$	$\left.\frac{\partial T}{\partial t}\right|_{diff}^{v\leftrightarrow lirs}$	$+$	$\left.\frac{\partial T}{\partial t}\right|_{diff}^{lr\leftrightarrow is}$	$+$	$\left.\frac{\partial T}{\partial t}\right|_{diff}^{diss}$	$+$	$\left.\frac{\partial T}{\partial t}\right|_{diff}^{gw}$
$\left.\frac{\partial T}{\partial t}\right|_{conv}$	$=$	$\left.\frac{\partial T}{\partial t}\right|_{conv}^{turb}$	$+$	$\left.\frac{\partial T}{\partial t}\right|_{conv}^{v\leftrightarrow lirs}$	$+$	$\left.\frac{\partial T}{\partial t}\right|_{conv}^{lr\leftrightarrow is}$	$+$	$\cancel{\left.\frac{\partial T}{\partial t}\right|_{conv}^{diss}}$	$+$	$\cancel{\left.\frac{\partial T}{\partial t}\right|_{conv}^{gw}}$
$\left.\frac{\partial T}{\partial t}\right|_{cloud}$	$=$	$\cancel{\left.\frac{\partial T}{\partial t}\right|_{cloud}^{turb}}$	$+$	$\left.\frac{\partial T}{\partial t}\right|_{cloud}^{v\leftrightarrow lirs}$	$+$	$\left.\frac{\partial T}{\partial t}\right|_{cloud}^{lr\leftrightarrow is}$	$+$	$\cancel{\left.\frac{\partial T}{\partial t}\right|_{cloud}^{diss}}$	$+$	$\cancel{\left.\frac{\partial T}{\partial t}\right|_{cloud}^{gw}}$
$\left.\frac{\partial q_v}{\partial t}\right|_{diff}$	$=$	$\left.\frac{\partial q_v}{\partial t}\right|_{diff}^{turb}$	$+$	$\left.\frac{\partial q_v}{\partial t}\right|_{diff}^{v\leftrightarrow lirs}$						
$\left.\frac{\partial q_v}{\partial t}\right|_{conv}$	$=$	$\left.\frac{\partial q_v}{\partial t}\right|_{conv}^{turb}$	$+$	$\left.\frac{\partial q_v}{\partial t}\right|_{conv}^{v\leftrightarrow lirs}$						
$\left.\frac{\partial q_v}{\partial t}\right|_{cloud}$	$=$	$\cancel{\left.\frac{\partial q_v}{\partial t}\right|_{cloud}^{turb}}$	$+$	$\left.\frac{\partial q_v}{\partial t}\right|_{cloud}^{v\leftrightarrow lirs}$						

Table 4: Physical processes contributing to the individual parametrization schemes. All processes that potentially contribute have been listed; those that are not presently implemented have been crossed out.

In addition to the run with CY32R3 presented above a run with CY32R1 was carried out. The results for the global estimates were the same within error margins (not demonstrated here in detail). This shows the relative insensitivity of the present estimates to the change in physical parametrization that has been implemented in the transformation from CY32R1 to CY32R3.

These results are further supported by a series of high-resolution T511 (40 km) short-range forecasts distributed over the year, where the forecasts remains very close to the analysis.

At the end it may be stressed again that this study has not intended to improve the concept of the Lorenz energy cycle in any way. Rather, it has tried, through implementing the indispensible sub-gridscale components, to bring the original concept to its completion.

A   Tendency contributions of the parametrization schemes

The parameterized tendencies (P_T and P_q) in the budget equations (14) and (15) have been split into contributions by the various parametrization schemes in equations (16) and (17). In turn these tendencies can be split into fractions acording to the underlying physical processes. Table 4 lists all these terms.

B   Flux contributions from the diffusion scheme

As pointed out in Section 4.3 and Appendix A the apparent tendencies of the state variables calculated by the individual parametrization schemes can be split into contributions due to turbulent transport, phase changes and in case of temperature also dissipation and gravity wave drag. However, dissipation and gravity wave drag were not stored in the diffusive tendency in this experiment (Table 2). The diffusion scheme also does not generate precipitation (i.e., no phase changes incorporating rain and snow). Hence the tendencies of temperature T, specific humidity q_v, liquid cloud water q_l and frozen cloud water q_i due to the diffusion scheme read (see Eqs. 20, 22 and Tab. 4):

$$\left.\frac{\partial T}{\partial t}\right|_{diff} = \left.\frac{\partial T}{\partial t}\right|_{diff}^{turb} + \left.\frac{\partial T}{\partial t}\right|_{diff}^{v\leftrightarrow l} + \left.\frac{\partial T}{\partial t}\right|_{diff}^{v\leftrightarrow i} + \left.\frac{\partial T}{\partial t}\right|_{diff}^{l\leftrightarrow i} \tag{41}$$

$$\left.\frac{\partial q_v}{\partial t}\right|_{diff} = \left.\frac{\partial q_v}{\partial t}\right|_{diff}^{turb} + \left.\frac{\partial q_v}{\partial t}\right|_{diff}^{v\leftrightarrow l} + \left.\frac{\partial q_v}{\partial t}\right|_{diff}^{v\leftrightarrow i} \tag{42}$$

$$\left.\frac{\partial q_l}{\partial t}\right|_{diff} = \left.\frac{\partial q_l}{\partial t}\right|_{diff}^{turb} + \left.\frac{\partial q_l}{\partial t}\right|_{diff}^{l\leftrightarrow v} + \left.\frac{\partial q_l}{\partial t}\right|_{diff}^{l\leftrightarrow i} \tag{43}$$

$$\left.\frac{\partial q_i}{\partial t}\right|_{diff} = \left.\frac{\partial q_i}{\partial t}\right|_{diff}^{turb} + \left.\frac{\partial q_i}{\partial t}\right|_{diff}^{i\leftrightarrow v} + \left.\frac{\partial q_i}{\partial t}\right|_{diff}^{i\leftrightarrow l} \tag{44}$$

For the phase change fractions the following relations should hold:

$$\left.\frac{\partial q_v}{\partial t}\right|_{diff}^{v\leftrightarrow l} = - \left.\frac{\partial q_l}{\partial t}\right|_{diff}^{l\leftrightarrow v} = -\frac{c_p}{L_v} \left.\frac{\partial T}{\partial t}\right|_{diff}^{v\leftrightarrow l} \tag{45}$$

$$\left.\frac{\partial q_v}{\partial t}\right|_{diff}^{v\leftrightarrow i} = - \left.\frac{\partial q_i}{\partial t}\right|_{diff}^{i\leftrightarrow v} = -\frac{c_p}{L_i} \left.\frac{\partial T}{\partial t}\right|_{diff}^{v\leftrightarrow i} \tag{46}$$

$$\left.\frac{\partial q_l}{\partial t}\right|_{diff}^{l\leftrightarrow i} = - \left.\frac{\partial q_i}{\partial t}\right|_{diff}^{i\leftrightarrow l} \tag{47}$$

$$\left.\frac{\partial T}{\partial t}\right|_{diff}^{l\leftrightarrow i} = -\frac{(L_i - L_v)}{c_p} \left.\frac{\partial q_l}{\partial t}\right|_{diff}^{l\leftrightarrow i} = \frac{(L_i - L_v)}{c_p} \left.\frac{\partial q_i}{\partial t}\right|_{diff}^{i\leftrightarrow l} \tag{48}$$

Adding Eqs. (43) and (44) to Eq. (42) and observing relations (45) to (47) yields:

$$\left.\frac{\partial q_v}{\partial t}\right|_{diff} + \left.\frac{\partial q_l}{\partial t}\right|_{diff} + \left.\frac{\partial q_i}{\partial t}\right|_{diff} = \left.\frac{\partial q_v}{\partial t}\right|_{diff}^{turb} + \left.\frac{\partial q_l}{\partial t}\right|_{diff}^{turb} + \left.\frac{\partial q_i}{\partial t}\right|_{diff}^{turb} \tag{49}$$

The tendencies on the left are from the one year experiment (Table 2). Thus the tendency due to the combined turbulent transport of q_v, q_l and q_i (right hand side of Eq. 49) can be calculated. Utilizing Eq. (27) the turbulent flux can be obtained.

Subtracting L_v/c_p (43) and L_i/c_p (44) from (41) and observing relations (45) to (48) yields:

$$\left.\frac{\partial T}{\partial t}\right|_{diff} - \frac{L_v}{c_p}\left.\frac{\partial q_l}{\partial t}\right|_{diff} - \frac{L_i}{c_p}\left.\frac{\partial q_i}{\partial t}\right|_{diff} =$$

$$\left.\frac{\partial T}{\partial t}\right|_{diff}^{turb} - \frac{L_v}{c_p}\left.\frac{\partial q_l}{\partial t}\right|_{diff}^{turb} - \frac{L_i}{c_p}\left.\frac{\partial q_i}{\partial t}\right|_{diff}^{turb} +$$

$$\left.\frac{\partial T}{\partial t}\right|_{diff}^{l\leftrightarrow i} - \frac{L_v}{c_p}\left.\frac{\partial q_l}{\partial t}\right|_{diff}^{l\leftrightarrow i} - \frac{L_i}{c_p}\left.\frac{\partial q_i}{\partial t}\right|_{diff}^{i\leftrightarrow l}$$

$$= \left.\frac{\partial T}{\partial t}\right|_{diff}^{turb} - \frac{L_v}{c_p}\left.\frac{\partial q_l}{\partial t}\right|_{diff}^{turb} - \frac{L_i}{c_p}\left.\frac{\partial q_i}{\partial t}\right|_{diff}^{turb} +$$

$$\left.\frac{\partial T}{\partial t}\right|_{diff}^{l\leftrightarrow i} - \frac{L_v}{c_p}\left.\frac{\partial q_l}{\partial t}\right|_{diff}^{l\leftrightarrow i} + \frac{L_i}{c_p}\left.\frac{\partial q_l}{\partial t}\right|_{diff}^{l\leftrightarrow i}$$

$$= \left.\frac{\partial T}{\partial t}\right|_{diff}^{turb} - \frac{L_v}{c_p}\left.\frac{\partial q_l}{\partial t}\right|_{diff}^{turb} - \frac{L_i}{c_p}\left.\frac{\partial q_i}{\partial t}\right|_{diff}^{turb} +$$

$$\left.\frac{\partial T}{\partial t}\right|_{diff}^{l\leftrightarrow i} + \left(\frac{L_i}{c_p} - \frac{L_v}{c_p}\right)\left.\frac{\partial q_l}{\partial t}\right|_{diff}^{l\leftrightarrow i}$$

$$= \left.\frac{\partial T}{\partial t}\right|_{diff}^{turb} - \frac{L_v}{c_p}\left.\frac{\partial q_l}{\partial t}\right|_{diff}^{turb} - \frac{L_i}{c_p}\left.\frac{\partial q_i}{\partial t}\right|_{diff}^{turb}$$

$$(50)$$

The tendencies on the left hand side are available from our experiment (Table 2). The right hand side comprises the combined apparent turbulent tendency of $T - L_v/c_p\, q_l - L_i/c_p\, q_i$ from which the related turbulent flux can be calculated.

Note: Only the sum of the turbulent transport tendencies on the right hand sides of Eqs. (49) and (50) can be calculated. This is because of the implementation of the diffusion scheme, where the turbulent transport is formulated for total water $q_t = q_v + q_l + q_i$ and liquid water static energy $s_l = gz + c_p T - L_v q_l - L_i q_i$ (ECMWF, 2007). It was decided to treat the turbulent transport of q_l and q_i as negligible. This is consistent with the implementation of the diffusion scheme, where the profiles of q_l and q_i are not altered by turbulent transport except for condensation due to supersaturation. Hence the turbulent fluxes calculated through vertical integration (Eq. (27)) of the turbulent tendencies (49) and (50) are considered as the kinematic turbulent fluxes of temperature F_{diff}^T and specific humidity $F_{diff}^{q_v}$ due to the diffusion scheme.

Acknowledgments

References

Arakawa, A., 2004: The Cumulus Parameterization Problem: Past, Present, and Future. *Journal of Climate*, **17**, 2493–2525.

Arpe, K., C. Brankovic, E. Oriol, and P. Speth, 1986: Variability in time and space of energetics from a long series of atmospheric data produced by ECMWF. *Beitr. Phys. Atmos.*, **59**, 321–355.

Bhatla, R., U. Mohanty, P. Raju, and O. Madan, 2004: A Study on Dynamic and Thermodynamic Aspects of Breaks in the Summer Monsoon over India. *Int. J. Climatol.*, **24**, 341–360.

Boer, G.J., 1975: Zonal and eddy forms of the available potential energy equations in pressure coordinates. *Tellus*, **27**, 433–443.

ECMWF, 2007: IFS documentation (CY31r1). ECMWF, http://www.ecmwf.int/research/ifsdocs/CY31r1/index.html.

Falk, G., and W. Ruppel, 1976: *Energie und Entropie. Eine Einführung in die Thermodynamik*. Springer, 408 pp.

Fortelius, C., 1995: Inferring the diabatic heat and moisture forcing of the atmosphere from assimilated data. *J. Climate*, **8**, 224–239.

Gill, A.E., 1982: *Atmosphere-Ocean Dynamics*, Volume 30 of *International Geophysics Series*. Academic Press, 662 pp.

Haimberger, L., and M. Hantel, 2000: Implementing convection into Lorenz's global cycle, Part II. A new estimate of the conversion rate into kinetic energy. *Tellus*, **52A**, 75–92.

Hamelbeck, F., L. Haimberger, and M. Hantel, 2001: Convection in PIDCAP. Part I: Evaluating LAM convection. *Meteorol. Atmos. Phys.*, **77**, 85–98.

Hantel, M., and H.R. Baader, 1978: Diabatic heating climatology of the zonal atmosphere. *J. Atmos. Sci.*, **35**, 1180–1189.

Hantel, M., M. Ehrendorfer, and L. Haimberger, 1993: A thermodynamic diagnostic model for the atmosphere. Part II: The general theory and its consequences. *Meteorol. Z., N.F.*, **2**, 255–271.

Hantel, M., and L. Haimberger, 2000: Implementing convection into Lorenz's global cycle. Part I: Gridscale averaging of the energy equations. *Tellus*, **52A**, 66–74.

Hantel, M., L. Haimberger, and F. Hamelbeck, 2001: Convection in PIDCAP Part II: DIAMOD – A standard for diagnosing convective quantities. *Meteorol. Atmos. Phys.*, **77**, 185–204.

Hortal, M., 2002: The development and testing of a new two-time-level semi-Lagrangian scheme (SETTLS) in the ECMWF forecast model. *Quart. J. Roy. Meteor. Soc.*, **128**, 1671–1687.

Hoskins, B.J., H.H. Hsu, I.N. James, M. Masutani, P.D. Sardeshmukh, and G.H. White, 1989: *Diagnostics of the global atmospheric circulation*. WCRP-27. WMO, 217 pp.

Johnson, D., 2000: Entropy, the Lorenz Energy Cycle, and Climate. In: *General Circulation Model Development. Past, Present, and Future*, D. Randall (Ed.), Volume 70 of *International Geophysics Series*, Chapter 22, pp. 659–720. Academic Press.

Kalnay, E., M. Kanamitsu, R. Kistler, W. Collins, D. Deaven, L. Gandin, M. Iredell, S. Saha, G. White, J. Woollen, Y. Zhu, M. Chelliah, W. Ebisuzaki, W. Higgins, J. Janowiak, K.C. Mo, C. Ropelewski, J. Wang, A. Leetmaa, R. Reynolds, R. Jenne, and D. Joseph, 1996: The NCEP/NCAR 40-year reanalysis project. *Bull. Amer. Meteorol. Soc.*, **77**, 437–471.

Li, L., A.P. Ingersoll, X. Jiang, D. Feldman, and Y.L. Yung, 2007: Lorenz energy cycle of the global atmosphere based on reanalysis datasets. *Geophys. Res. Lett.*, **34**, L16813.

Lorenz, E.N., 1955: Available potential energy and the maintenance of the general circulation. *Tellus*, **7**, 157–167.

Lorenz, E.N., 1967: *The Nature and Theory of the General Circulation of the Atmosphere*. WMO–No.218.TP.115. World Meteorological Organization, 161 pp.

Newell, R.E., D.G. Vincent, T.G. Dopplick, D. Ferruzza, and J.W. Kidson, 1970: The energy balance of the global atmosphere. In: *The Global Circulation of the Atmosphere*, G. A. Corby (Ed.), pp. 42–90. London: Roy. Met. Soc.

Oort, A.H., 1964: On estimates of the atmospheric energy cycle. *Mon. Wea. Rev.*, **92**, 483–493.

Oort, A.H., 1983: *Global Atmospheric Circulation Statistics, 1958-1973*, Volume 14 of *NOAA Professional Paper*. U.S. Department of Commerce/NOAA, 180 pp.

Oort, A.H., and J.P. Peixóto, 1983: Global angular momentum and energy balance requirements from observations. *Adv. Geophys*, **25**, 355–490.

Oort, A.H., and E.M. Rasmusson, 1971: *Atmospheric Circulation Statistics*, Volume 5 of *NOAA Professional Paper*. U.S. Department of Commerce/NOAA, 323 pp.

Peixóto, J.P., and A.H. Oort, 1992: *Physics of Climate*. American Institute of Physics, 520 pp.

Ritchie, H., C. Temperton, A. Simmons, M. Hortal, T. Davies, D. Dent, and M. Hamrud, 1995: Implementation of the semi–Lagrangian method in a high–resolution version of the ECMWF forecast model. *Mon. Wea. Rev.*, **123**, 489–514.

Rosen, R.D., 1999: The global energy cycle. In: *Global Energy and Water Cycles*, K. A. Browning and R. J. Gurney (Eds.), Chapter 1.1, pp. 1–9. Cambridge University Press.

Siegmund, P., 1994: The generation of available potential energy, according to Lorenz' exact and approximate equations. *Tellus*, **46A**, 566–582.

Simmons, A.J., and D.M. Burridge, 1981: An energy and angular–momentum conserving vertical finite-difference scheme and hybrid vertical coordinates. *Mon. Wea. Rev.*, **109**, 758–766.

Stull, R.B., 1988: *An Introduction to Boundary Layer Meteorology*. Atmospheric Sciences Library. Kluwer Academic Publishers, 666 pp.

Uppala, S.M., P.W. Kållberg, A.J. Simmons, U. Andrae, V. da Costa Bechtold, M. Fiorino, J.K. Gibson, J. Haseler, A. Hernandez, G.A. Kelly, X. Li, K. Onogi, S. Saarinen, N. Sokka, R.P. Allan, E. Andersson, K. Arpe, M.A. Balmaseda, A.C.M. Beljaars, L. van de Berg, J. Bidlot, N. Bormann, S. Caires, F. Chevallier, A. Dethof, M. Dragosavac, M. Fisher, M. Fuentes, S. Hagemann, E. Hólm, B.J. Hoskins, L. Isaksen, P.A.E.M. Janssen, R. Jenne, A.P. McNally, J.F. Mahfouf, J.J. Morcrette, N.A. Rayner, R.W. Saunders, P. Simon, A. Sterl, K. Trenberth, A. Untch, D. Vasiljevic, P. Viterbo, and J. Woollen, 2005: The ERA-40 Re-analysis. *Quart. J. Roy. Meteor. Soc.*, **131**, 2961–3012.

van Mieghem, J., 1973: *Atmospheric Energetics*. Oxford Monogr. on Meteorology. Clarendon Press, 306 pp.

Yanai, M., and R.H. Johnson, 1993: Impacts of cumulus convection on thermodynamic fields. In: *The representation of cumulus convection in numerical models*, K. A. Emanuel and D. J. Raymond (Eds.), Volume 24 of *Meteorological Monographs*, pp. 39–62. Boston, Massachusetts: American Meteorological Society.